Structures of Tetrafluorocyclopropene, Hexafluorocyclobutene, Octafluorocyclopentene and Related Perfluoroalkene Radical Anions Revealed by Electron Spin Resonance Spectroscopic an...

ARTICLE *in* THE JOURNAL OF PHYSICAL CHEMISTRY A · JUNE 2006

Impact Factor: 2.69 · DOI: 10.1021/jp0602427 · Source: PubMed

Structures of Tetrafluorocyclopropene, Hexafluorocyclobutene, Octafluorocyclopentene and Related Perfluoroalkene Radical Anions Revealed by Electron Spin Resonance Spectroscopic and Computational Studies

Masaru Shiotani*,†

Department of Applied Chemistry, Graduate School of Engineering, Hiroshima University, Higashi-Hiroshima 739-8527, Japan

Petter Persson† and Sten Lunell†

Department of Quantum Chemistry, Uppsala University, S-751 20 Uppsala, Sweden

Anders Lund†

Department of Physics, Chemistry and Biology, Linköping University, S-581 83 Linköping, Sweden

Ffrancon Williams†

Department of Chemistry, University of Tennessee, Knoxville, Tennessee 37996-1600

Received: January 13, 2006; In Final Form: March 10, 2006

Isotropic and anisotropic ESR spectra were observed for the radical anions of hexafluorocyclobutene (*c*-$C_4F_6^-$), octafluorocyclopentene (*c*-$C_5F_8^-$) and perfluoro-2-butene ($CF_3CF{=}CFCF_3^-$) in γ-irradiated plastically crystalline neopentane, tetramethylsilane (TMS) and TMS-d_{12} matrices, or the rigid 2-methyltetrahydrofuran (MTHF) matrix. The isotropic spectra of *c*-$C_4F_6^-$ and *c*-$C_5F_8^-$ are characterized by three different sets of pairs of ^{19}F nuclei with the isotropic hyperfine (hf) splittings of 15.2 (2F), 6.5 (2F), 1.1 (2F) mT for *c*-$C_4F_6^-$ and 14.7 (2F), 7.4 (2F), 1.0 (2F) mT for *c*-$C_5F_8^-$. By comparison with the results of ab initio quantum chemical computations, the large triplet ^{19}F hf splittings of ca. 15 mT are assigned to the two fluorines attached to the C=C bond. The UHF, B3LYP and MP2 computations predict that the geometrical structures of the perfluoroalkenes are strongly distorted by one-electron reduction to form their radical anions; *c*-$C_3F_4^-$: C_2 symmetry (^{2}A state) ← C_{2v} ($^1A_1$), *c*-$C_4F_6^-$: C_1 (^{2}A) ← C_{2v} ($^1A_1$) and *c*-$C_5F_8^-$: C_1 (^{2}A) ← C_s ($^1A'$). The structural distortion arises from a mixing of the π^* and higher-lying σ^* orbitals at the C=C carbons similar to that previously found for $CF_2{=}CF_2^-$ with a C_{2h} distortion. The isotropic ^{19}F hf splittings computed with the B3LYP method with 6-311+G(2df,p) basis set for the geometry optimized by the UHF and/or MP2 methods are within 6% error of the experimental values. The experimental anisotropic spectra of *c*-$C_4F_6^-$, *c*-$C_5F_8^-$ and $CF_2{=}CF_2^-$ were satisfactorily reproduced by the ESR spectral simulation method using the computed hf principal values and orientation of ^{19}F nuclei. In addition, the electronic excitation energies and oscillator strengths for the $CF_2{=}CF_2^-$, *c*-$C_3F_4^-$, *c*-$C_4F_6^-$ and *c*-$C_5F_8^-$ radical anions were computed for the first time by TD-DFT methods.

1. Introduction

The physical and chemical properties of perfluorocarbons have attracted much attention not only in terms of their intrinsic molecular character but also for the development of promising materials for industrial applications. Perfluorocarbons have remarkable properties such as chemical inertness, thermal stability, high hydrophobicity, low dielectric constant, and large electronegativity; these properties have led to their widespread use in many commercial products such as blood substitutes, pharmaceuticals, surface modifiers, lubricants, sealants, oxygen carriers, and inert solvents among many other examples.[1,2] Furthermore, perfluorocarbons have been widely employed as etchants for semiconductor fabrication.[3,4] These applications in modern technology require a deeper understanding of the electronic structure and reactivity of fluorocarbons. For example, the elementary reactions that occur in the use of etchant perfluorocarbons involve the fundamental physical and chemical processes that accompany electron excitation and electron capture in high-temperature plasmas.[5,6] However, the detailed electronic structures of perfluorocarbon radical ions, especially radical anions, have not yet been fully characterized.

Electron spin resonance (ESR) spectroscopy is one of the best experimental methods to study radical ions because of its high specificity and sensitivity; moreover, the technique can provide direct information on the electronic structure of the radical ions as well as information on their participation in elementary chemical reactions. In particular, detailed ESR studies on perfluorocycloalkane radical anions (*c*-$C_nF_{2n}^-$ with $n = 3-5$) previously carried out by two of the present authors[7−9] have shown that these radical anions have isotropic ^{19}F hyperfine

† E-mail: M.S., mshiota@hiroshima-u.ac.jp; P.P., petter.persson@kvac.uu.se; S.L., lunell@kvac.uu.se; A.L., alund@ifm.liu.se; F.W., williams@ion.chem.utk.edu.

10.1021/jp0602427 CCC: $33.50
Published on Web 04/27/2006

(hf) patterns corresponding to a set of completely equivalent fluorines for each radical anion. Moreover, the isotropic ^{19}F hf splittings decrease with increasing ring size such that the sum of the ^{19}F isotropic splittings remains nearly constant along the series for $n = 3-5$. This suggests an important concept of "electron delocalization" in these *saturated* perfluorocycloalkane radical anions. Recently, ElSohly et al.[9] computed the structures *of* c-$C_nF_{2n}^-$ ($n = 3-5$) using the B3LYP DFT method and demonstrated good agreement between the calculated and experimental values for the ^{13}C and ^{19}F hf splitting constants. Taken together, these results clearly establish that the SOMO (singly occupied molecular orbital) is delocalized in a π-like arrangement of antibonding C−F σ^* orbitals distributed over the equivalent fluorines of a time-averaged D_{nh} ($n = 3-5$) structure.[9] Corroboration of this unusual finding comes from an independent theoretical study of these perfluorocycloalkanes,[6] which also concludes that the unpaired electron is delocalized "in the multiatom SOMOs of the three- to five-membered ring anions".

In contrast, ESR and computational studies on *unsaturated* perfluorocarbon radical anions are in general rather limited,[10−25] although neutral fluorinated hydrocarbon radicals[26−32] and radical cations[33−40] have been studied extensively. Specifically, no combined ESR and theoretical studies have hitherto been carried out on perfluoroalkene radical anions except for the parent tetrafluoroethylene species ($CF_2{=}CF_2^-$)[10−18] and its monochloro, monobromo and dihydro derivatives,[19,20] although several related studies of the hexafluorobenzene radical anion have been reported.[21−25] In an early contribution,[10] two of the present authors reported the isotropic ^{13}C and ^{19}F hf splittings of $CF_2{=}CF_2^-$ and also described the anisotropic ESR spectra. Subsequently, Paddon-Row et al. computed the geometry of $CF_2{=}CF_2^-$ by ab initio UHF computations with 3-21G basis set and reported that the radical anion has a distorted anti-bent structure with C_{2h} symmetry.[13] Furthermore, Shchegoleva et al. showed that INDO calculations of the ^{19}F hf splittings also support a chair (C_{2h}) structure resulting from the out-of-plane distortions induced by the pseudo-Jahn−Teller interaction of the ground π^* state with the higher-lying excited (^2A_g) σ^* state in the planar species.[15] The anisotropic ESR line shape of $CF_2{=}CF_2^-$ has also been discussed on the basis of semiempirical INDO computations.[14] However, these latter calculations lacked sufficient precision to predict the geometrical parameters as well as the anisotropic ^{19}F hf splittings.

In the present paper we report the electronic and geometrical structures of perfluorocycloalkene radical anions. We first describe the ESR spectra of hexafluorocyclobutene (c-$C_4F_6^-$) and octafluorocyclopentene (c-$C_5F_8^-$) radical anions generated in the plastically crystalline neopentane and TMS matrices,[7,8,10,11] whereas the anisotropic spectra were obtained in the rigid 2-methyltetrahydrofuran (MTHF) matrix. As a suitable reference, the isotropic spectrum of $CF_3CF{=}CFCF_3^-$ is also reported. In addition, previous experimental works on $CF_2{=}CF_2^-$ [10−12] and tetrafluorocyclopentene (c-$C_3F_4^-$) radical anion[41] are reviewed and newly considered in the light of our present computational results on these species. For this comparison, we are indebted to Dr. M. B. Yim for providing us with the unpublished values of the experimental ^{19}F hf splittings for c-$C_3F_4^-$.[41]

In complementary studies, the geometrical structures and isotropic ^{19}F hf splittings have been computed by the B3LYP and the ab initio MP2 and UHF theoretical methods. Comparison of the experimental isotropic ^{19}F splittings with the computed values allows the assignment of ^{19}F splittings and a discussion of the structural distortion of c-$C_nF_{2n-2}^-$ for $n = 3-5$ with regard to their corresponding SOMOs. Furthermore, we show that the anisotropic ESR spectra of c-$C_4F_6^-$, c-$C_5F_8^-$ and $CF_2{=}CF_2^-$ computed using the theoretical ^{19}F hf principal values and principal directions agree quite well with the experimental anisotropic ones. On the basis of these results, we conclude that an anti-bent type of structural distortion similar to $CF_2{=}CF_2^-$ occurs also for perfluorocycloalkenes (c-C_nF_{2n-2}) with $n = 3-5$ after undergoing one-electron reduction. Finally, the theoretical electronic excitation energies and oscillator strengths for the $CF_2{=}CF_2^-$, c-$C_3F_4^-$, c-$C_4F_6^-$ and c-$C_5F_8^-$ radical anions are reported for the first time.

2. Experimental and Computational Methods

Materials. Hexafluorocyclobutene (c-C_4F_6) and octafluorocyclopentene (c-C_5F_8) used in this study were obtained from Peninsular Chem. Research (PCR, Inc.). Perfluoro-2-butene ($CF_3CF{=}CFCF_3$) was obtained from Matheson Gas Products and Pfaltz & Bauer; the minimum purity was stated to be 97% on the basis of the content of the trans-isomer. The other chemicals used were neopentane (2,2-dimethylpropane; Neop.; $C(CH_3)_4$) from Matheson, tetramethylsilane (TMS; $Si(CH_3)_4$) from either Mallinckrodt or the Norell Chemical Co., tetramethylsilane-d_{12} (TMS-d_{12}; $Si(CD_3)_4$) from Merck Sharp and Dohme Ltd., and 2-methyltetrahydrofuran (MTHF) from Eastman Organic Chemicals. *N*,*N*,*N*′,*N*′-Tetramethyl-*p*-phenylenediamine (TMPD) was supplied by Eastman as the dihydrochloride.

ESR Samples and Measurements. The general methods of sample preparation, γ-ray irradiation (from ^{60}Co source), and ESR spectral measurements have been described in previous publications.[7−11] In brief, the perfluoroalkene radical anions were generated by γ-ray irradiation at 77 K of solid solutions containing ca. 1 mol % of the perfluoroalkene in the solid neopentane, TMS, TMS-d_{12} or MTHF matrix. The "isotropic" spectra were observed using the three tetramethyl derivatives which are often described as rotator or plastically crystalline matrices; the radicals trapped in these plastic phases at higher temperature are stable enough to be observed by ESR.[27] The typical γ-irradiation dose was ca. 10 kGy. Photoionization of TMPD in solid matrices, which is another method of generating radical anions, was carried out at 320 nm using filtered light (Corning 7740 and 9863 filters) from a 1 kW BH-6 arc mercury lamp. The ESR spectra were generally recorded after irradiation at temperatures up to the disappearance points of the radical anions using the Varian (V-4502−15) or JEOL (JES-RE1X) X-band spectrometers operating at 100 kHz modulation and at variable temperatures regulated by an ESR 900 Oxford continuous flow cryostat. The field strength was measured using a proton magnetic resonance probe (NMR Gaussmeter, model 1037). The photobleaching experiments were carried out using unfiltered light from a tungsten lamp.

Computations. Quantum chemical computations were performed to compare the ESR ^{13}C and ^{19}F hyperfine (hf) splittings and to provide information on the electronic structures of the radical anions. The Gaussian 03 suite of programs were used for quantum chemical computations and the abbreviations relating to the computations are taken from this program package.[42] The B3LYP, MP2 and UHF methods were used for geometry optimizations with the 6-31+G(d,p) and 6-311+G(d,p) basis sets. Furthermore, both the B3LYP and MP2 methods were used to compute the ESR hf splittings with the 6-31+G(2df,p) and 6-311+G(2df,p) basis sets for the optimized structures. Excitation energies and oscillator strengths of the

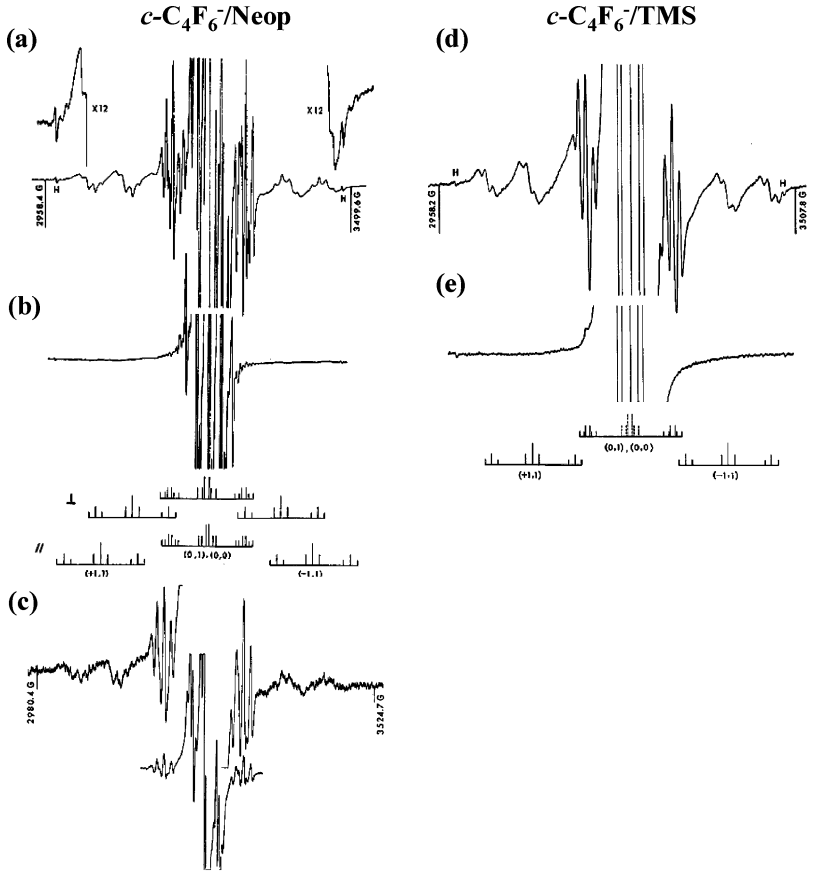

Figure 1. (a)−(c) X-band ESR spectra of a 77 K γ-irradiated solid solution of 1 mol % *c*-C_4F_6 in neopentane (Neop). (a) and (b) were recorded at 133 K before and after exposing the sample to unfiltered light from a tungsten lamp (ν = 9121.7 Hz). (c) was recorded at 130 K for a UV-illuminated solid solution of 1 mol % TMPD and 1 mol % *c*-C_4F_6 in Neop (ν = 9119.5 Hz). (d) and (e) ESR spectra of a 77 K γ-irradiated solid solution of 1 mol % *c*-C_4F_6 in tetramethylsilane (TMS). (d) and (e) were recorded at 138 K before and after exposing the sample to unfiltered light from a tungsten lamp (ν = 9116.9 Hz). The line diagram shows the expected positions of the second-order ^{19}F hyperfine lines calculated from the parameters listed in Table 1 for the *c*-$C_4F_6^-$ radical anion. The values in parentheses, (+1, 0) etc., correspond to (M_I, I), where I is the total nuclear spin and M_I is its *z*-component.

radical anions were computed by the TD (time-dependent) B3LYP methods with the 6-311+G(d,p) basis set. For "powder" ESR spectral simulations, the homemade program "Xfit" was employed.[43,44]

3. Results and Discussion

3.1. Isotropic ESR Spectra.

Hexafluorocyclobutene Radical Anion (c-$C_4F_6^-$). Figure 1a shows the ESR spectrum of *c*-$C_4F_6^-$ in neopentane (Neop) recorded at 133 K, the observed ^{19}F hyperfine (hf) pattern lying outside the intense central band due to the matrix radicals. The spectrum is close to being isotropic but, on closer analysis, is found to retain a definite residual anisotropy. The spectrum can be analyzed in terms of a radical possessing three different sets of pairs of ^{19}F nuclei. One pair of ^{19}F atoms accounts for the largest hf splitting with axial symmetry, and the other two sets of ^{19}F pairs give rise to the smaller isotropic splittings. The line diagram shows the parallel and perpendicular components with the expected positions of the second-order hf lines,[30,45,46] as calculated from $A_{||}$ =18.8 and $A_\perp$ = 13.2 mT (two equivalent ^{19}F nuclei) together with the values of the other smaller ^{19}F hf splittings given in Table 1. As shown in Figures 1d and 2d, the completely isotropic spectrum of *c*-C_4F_6 was successfully observed when the matrix was changed to TMS or TMS-d_{12}, the isotropic ^{19}F hf splittings being 15.2 (2F), 6.51 (2F) and 1.09 (2F) mT (Table 1). These results were not unexpected because it is well-known that the neopentane and TMS matrices give rise to "rotator" solids that are suitable for the observation of nearly isotropic EPR spectra from small and highly symmetrical radicals,[7,8,10,11] and it is likely that the rotation of methyl groups about the C−C (Neop) or C−Si (TMS) bond can accelerate the rotational diffusion and hence the tumbling rates of the radical trapped in the matrix molecules. In the absence of structural information, the positional assignment of the hf splittings due to the three ^{19}F pairs in *c*-$C_4F_6^-$ is not straightforward on strictly empirical grounds. However, comparison of these splittings with the computed values for the theoretically derived structure of lowest energy allows a firm identification to be made, as shown in a later section.

All the spectral lines attributable to *c*-$C_4F_6^-$ in Neop and TMS were completely removed by exposure of the sample to unfiltered light from a tungsten lamp as shown in Figure 1b,e. This photobleaching result not only is consistent with the assignment of the lines to a single species but also supports the anionic nature of the radical, as will be described in the later section on "Electronic Spectra". Furthermore, the ESR spectral assignment and identification of the *c*-$C_4F_6^-$ radical anion were further established experimentally by the generation of an identical spectrum by TMPD photoionization, this being an alternative and highly specific method of radical anion formation. As shown by a comparison of spectrum c with spectrum a, the same ^{19}F hf structure is clearly displayed despite the lower signal-to-noise ratio.

TABLE 1: ESR Parameters of Some Perfluorocycloalkene and Related Radical Anions

radical anion	matrix[a]	*T*/K	*g* value	^{19}F-hf splitting/mT	note
c-$C_3F_4^-$	TMS-d_{12}	142	2.0047	$A_{\|}(2F) = 20.1$, $A_{\perp}(2F) = 18.4$ {$a(2F) = 18.9$}	ref 41; Figure 8
	2-MTFH	86	$g_{\|} = 2.0045$ $g_{\perp} = 2.0058$	$A_{\|}(2F) = 26.5$, $A_{\perp}(2F) = 14.3$ {a (2F) = 18.4}	
c-$C_4F_6^-$	Neop	133	2.0038	$a_1(2F) = 15.1$,[b] $a_2(2F) = 6.5$, $a_3(2F) = 1.2$	Figures
	TMS-d_{12}	167	2.0030	$a_1(2F) = 15.2$, $a_2(2F) = 6.5$, $a_3(2F) = 1.1$	1, 2 & 9
c-$C_5F_8^-$	Neop	130	2.0031	$a_1(2F) = 15.0$, $a_2(2F) = 7.4$	Figures
	TMS-d_{12}	168	2.0027	$a_1(2F) = 14.7$, $a_2(2F) = 7.4$, $a_3(2F) = 1.0$	3 & 10
$CF_3CF{=}CFCF_3^-$	TMS	134	2.0027	$a_1(2F) = 16.93$, $a_2(6F) = 2.56$	Figure 4
$CF_2{=}CF_2^-$	TMS-d_{12}	120	2.0027	$a(4F) = 9.43$, $a(^{13}C) = 4.87$	ref 10;
	MTHF	83		$A_{\|}(4F) = 13.59$, $A_{\perp}(2F) = 7.44$ {$a(4F) = 9.49$}	Figure 11

[a] Neop: neopentane, $C(Me)_4$. TMS: tetramethylsilane, $Si(Me)_4$. TMS-d_{12}: perdeuterotetramethylsilane, $Si(Me\text{-}d_3)_4$. MTHF: 2-methylhydrofuran. [b] Isotropic value calculated from the measured splittings of $A_{\|} = 18.81$ and $A_{\perp} = 13.18$ mT for a spectrum showing residual hf anisotropy.

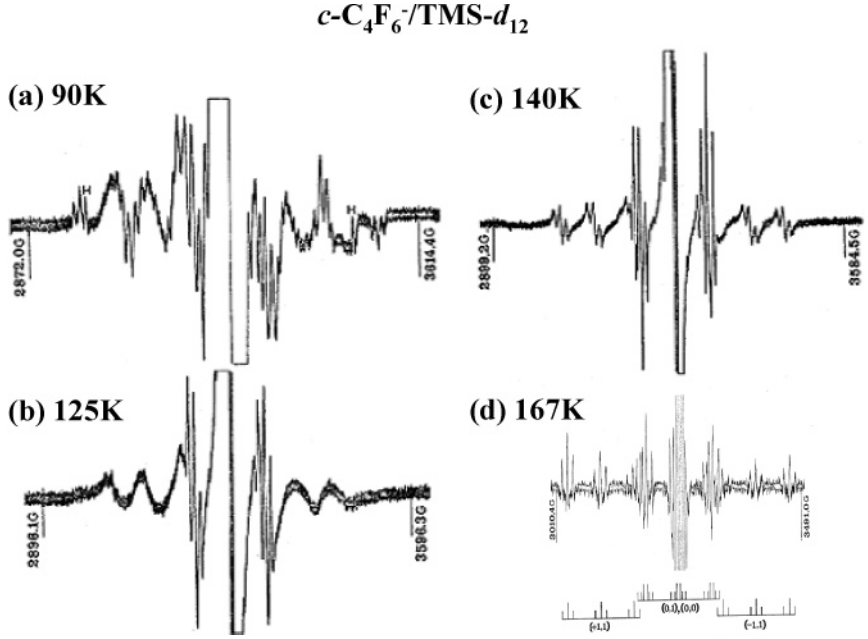

Figure 2. (a)−(c) Temperature-dependent first derivative ESR spectra of *c*-$C_4F_6^-$ in TMS-d_{12} between 90 and 140 K (ν = 9121.4 Hz). The *c*-$C_4F_6^-$ radical was generated by γ-ray irradiation of the solid solution of 1 mol % *c*-C_4F_6 in TMS-d_{12} at 77 K. The spectra were recorded at the same gain. (d) Second derivative ESR spectrum of *c*-$C_4F_6^-$ in TMS-d_{12} at 167K (ν = 9121.4 Hz). The line diagram shows the expected positions of the second-order ^{19}F hyperfine lines calculated from the parameters listed in Table 1 for the *c*-$C_4F_6^-$ radical anion.

Figure 2 shows the temperature-dependent ESR spectra of *c*-$C_4F_6^-$ in TMS-d_{12} taken between 90 and 167 K. An advantage of the TMS-d_{12} over the TMS matrix is that it provides spectra of much higher resolution. In addition to providing ESR spectra with a narrower line width, the use of TMS-d_{12} has the desirable effect of decreasing the spectral width of the matrix radical which otherwise seriously masks the central portion of the spectrum in the γ-irradiated samples.[10,11] The second-derivative ESR spectrum (Figure 2d) was recorded at 167 K to resolve the second-order ^{19}F hf splitting of the signals due to the $I = 0$ and $I = 1$ species, especially at the $M_I = 0$ band, so that the present identification of the spectral lines was reconfirmed and the "precise" isotropic hf splittings obtained, where I and M_I represent the total nuclear spin state of the two fluorine nuclei involved (with the largest hf splitting) and their *z*-component, respectively. Upon cooling the sample from 140 to 125 K, the spectral lines became broader, especially at both of the outer $M_I = \pm 1$ lines. Upon decreasing the temperature to 90 K, the two outer lines move further outward and concomitantly the spectrum changes to a complicated structure with many lines and a narrower line width as can be seen in spectrum a. At the same time the total splitting increased from 30.4 mT (140 and 167 K) to 59.1 mT (90 K). The spectral change upon cooling can be reasonably attributed to the transition from the isotropic to the anisotropic spectrum. The spectrum at 90 K can, in fact, be successfully interpreted as that expected in the rigid limit; this was accomplished by means of a spectral simulation using the computed principal values and directions of the ^{19}F hf coupling tensors, as will be mentioned in the section on "Anisotropic ESR Spectra".

Octafluorocyclopentene Radical Anion (c-$C_5F_8^-$). Figure 3a shows the ESR spectrum of *c*-$C_5F_8^-$ radiolytically generated in the TMS matrix and recorded at 162 K. The spectrum is essentially isotropic, but the spectral resolution is inferior to that of *c*-$C_4F_6^-$ in TMS recorded at 140 K. The resolution was again much improved when the matrix was changed to TMS-d_{12}, as shown by the second-derivative isotropic spectrum of *c*-$C_5F_8^-$ in Figure 3c, observed and recorded at 224 K. It is noticeable, however, that this improvement in spectral resolution is marked by a relatively large temperature difference (224 vs 162 K) between the optimized spectra, each having been recorded at the respective high-temperature limit in the two

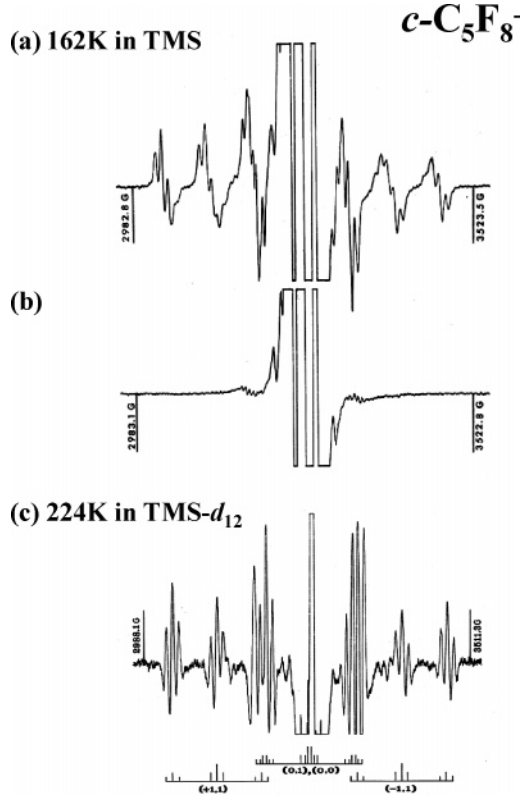

Figure 3. (a) and (b) First derivative ESR spectra of a γ-irradiated solid solution of 1 mol % c-C_5F_8 in TMS. (a) and (b) were recorded at 162 K before and after exposing the sample to unfiltered light from a tungsten lamp (ν = 9113.9 Hz). (c) Second derivative ESR spectrum of c-$C_5F_8^-$ in TMS-d_{12} at 224 K (ν = 9112.9 Hz). The line diagram shows the expected positions of the second-order ^{19}F hyperfine lines calculated from the parameters listed in Table 1 for the c-$C_5F_8^-$ radical anion.

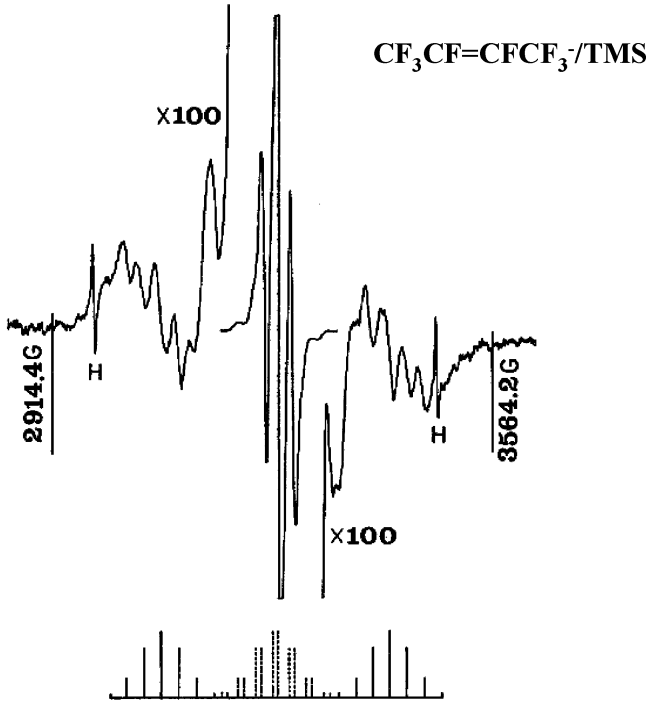

Figure 4. First derivative ESR spectrum of a γ-irradiated solid solution of 1 mol % perfluoro-2-butene ($CF_3CF{=}CFCF_3$) in TMS recorded at 134 K (ν = 9104.7 Hz). The line diagram shows the expected positions of the second-order ^{19}F hyperfine lines calculated from the parameters listed in Table 1 for the $CF_3CF{=}CFCF_3^-$ radical anion.

matrices before radical anion decay sets in. This result can therefore be simply attributed to the fact that the disappearance temperature of the radical anion is much higher in TMS-d_{12} than in TMS, thereby allowing for a greater motional narrowing to occur in the former case. Accordingly, this temperature effect could well be the main reason for the improved resolution of the c-$C_5F_8^-$ spectrum in TMS-d_{12}, in addition to the reduced magnetic moment of ^{2}H compared to ^{1}H as noted previously.

The observed spectrum is again characteristic of a radical possessing three different pairs of ^{19}F nuclei. The observed isotropic ^{19}F hf splittings are 14.7 (2F), 7.4 (2F) and 1.0 (2F) mT in TMS-d_{12}, the values being quite close to those of c-$C_4F_6^-$ (Table 1). The assignment of the ^{19}F hf splittings will be made by comparing them with the computed ones by DFT methods in a later section. As with c-$C_4F_6^-$, all the spectral lines attributable to c-$C_5F_8^-$ in TMS were also completely removed by exposure of the sample to unfiltered light from a tungsten lamp as shown in Figure 3b. The anisotropic spectrum generated in rigid MTHF matrix will be discussed by comparing it with the computed spectrum in a later section.

Perfluoro-2-butene Radical Anion ($CF_3CF{=}CFCF_3^-$). To compare its electronic structure with those of the perfluorocycloalkene radical anions (c-$C_nF_{2n-2}^-$ with n = 3−5), the $CF_3CF{=}CFCF_3^-$ radical anion was generated in the irradiated TMS matrix at 77 K and subjected to an ESR study. An isotropic spectrum of $CF_3CF{=}CFCF_3^-$ was observed at elevated temperatures, as shown in Figure 4. The spectrum consists of a triplet of septets with isotropic ^{19}F hf splittings of 16.93 mT (two magnetically equivalent ^{19}F atoms) and 2.56 mT (six ^{19}F atoms) at 134 K (Table 1). Identification of the experimental hf splittings in this case is quite straightforward, because the larger splitting of 16.93 mT is clearly attributable to the two ^{19}F atoms attached to the C=C bond whereas the smaller splitting of 2.56 mT can be assigned to the six ^{19}F atoms belonging to the two CF_3 groups undergoing free rotation. The geometrical and electronic structures of $CF_3CF{=}CFCF_3^-$ will be discussed by comparing the experimental ^{19}F hf splittings with the computed ones in the next section.

3.2. Computational Results: Geometry, SOMO and ^{19}F Hyperfine Splittings.

Tetrafluorocyclopropene: c-C_3F_4 and c-$C_3F_4^-$. The neutral c-C_3F_4 molecule has a C_{2v} point-group geometry with a $^1A_1$ electronic ground state. Its molecular structure has been studied by X-ray crystallography and in the gas phase by a combined analysis of electron-diffraction data, microwave and ^{19}F NMR spectra.[47] The geometrical parameters are in good agreement with those obtained in the present ab initio study by the B3LYP, MP2 and UHF methods, all with 6-311+G(d,p) basis set (the computed geometrical parameters can be found in Supporting Information 1). The computations predict that a significant and large geometrical distortion occurs when one electron is added to c-C_3F_4 to form c-$C_3F_4^-$, as seen in Figure 5b. The C=C, =C−F and −C−F bond lengths increase by at least 0.08, 0.1 and 0.04 Å, respectively, and the C−C bond length contracts by at least 0.02 Å. The changes in the bond angles are more prominent. The fluorine atom attached to the C=C bond deviates from the molecular plane by at least 20.2°. Moreover, the ∠C=C−C and ∠C=C−F bond angles contract by at least 2 and 19°, respectively. The optimized geometrical parameters depend very little on the method, the bond lengths differing by no more than 0.1 Å, and the bond angles by no more than 0.4° when different methods are used, except for the deviation of ±1.2° in the displacement of the bent C−F bond from the molecular plane.

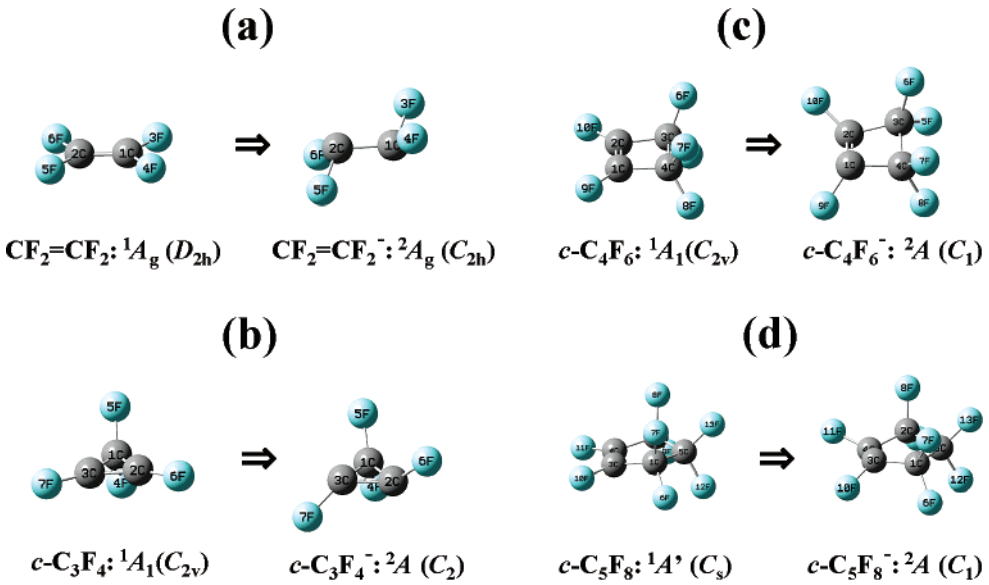

Figure 5. Geometrical structures of the perfluoroalkenes before and after one electron reduction together with ground electronic states and point group symmetries (in parentheses).

The ^{19}F hyperfine splittings computed for c-$C_3F_4^-$ are summarized in Table 2. Hereinafter we use the following abbreviation; "B3LYP/6-311+G(2df,p)//MP2/6-311+G(d,p)" for "ESR hyperfine parameter computations by the B3LYP method (with 6-311+G(2df,p) basis set) for the geometry optimized by the MP2 method (with 6-311+G(d,p) basis set)", etc. The computations were carried out by four different methods:

method A: B3LYP/6-311+G(2df,p)//B3LYP/6-311+G(d,p)
method B: MP2/6-311+G(2df,p)//MP2/6-311+G(d,p)
method C: B3LYP/6-311+G(2df,p)//MP2/6-311+G(d,p)
method D: B3LYP/6-311+G(2df,p)//UHF/6-311+G(d,p)

The electronic ground state of c-$C_3F_4^-$ is ^{2}A in C_2 symmetry at all method levels (Figure 5b). The computed isotropic ^{19}F hf splitting of the two "α"-fluorines attached to the C=C bond is in excellent agreement with the experimental one of 18.4 mT (for two equivalent ^{19}F atoms).[41] Consistent with the experimental results, the splittings computed for the pair of ^{19}F atoms at carbon C1 are too small to be resolved in low temperature "powder" spectra; the line width being more than ca. 0.6 mT in general. Errors relative to the experimental isotropic ^{19}F hf splitting of c-$C_3F_4^-$ in Table 2 range from 0.5% (method C) to 5% (methods B and D). The computed anisotropic ^{19}F hf splittings cannot be directly compared with the experimental ones as will be mentioned in the section of "Anisotropic ESR Spectra". Figure 6b shows the singly occupied molecular orbital (SOMO) projected to the $x-y$ plane, where the y-axis is parallel to the C2=C3 bond and the x-axis is perpendicular to the molecular plane. As a result of geometrical distortions, the majority of the unpaired electron spin density lies in the sp^3-like hybrid orbitals of the two olefin carbon atoms formed by the π^* and σ^* orbital mixing, as will be discussed in a later section. The ^{19}F hf splittings computed for c-$C_3F_4^-$ with the geometrical structure forced to the original C_{2v} symmetry are also listed as a reference in Table 2a.

Hexafluorocyclobutene: c-C4F6 and c-C4F6⁻. The neutral c-C_4F_6 molecule has a C_{2v} point-group geometry with a $^1A_1$ electronic ground state. Its molecular structure has been studied in the gas phase by electron-diffraction and microwave spectroscopy.[48,49] As with c-C_3F_4, the geometrical parameters are in rather good agreement with those obtained in the present ab initio study (the computed geometrical parameters can be found in Supporting Information 2). The computations predict again a significant geometrical distortion, as in the c-$C_3F_4^-$ anion, when one electron is added to c-C_4F_6 to form c-$C_4F_6^-$; see Figure 5c. The C=C, =C−F and −C−F bond lengths increase by at least 0.07, 0.08 and 0.03 Å, respectively and the C−C bond length contracts by at least 0.02 Å. The ∠C=C−C and ∠C=C−F bond angles contract by at least 2.9 and 9.1°, respectively. Moreover, the C−C=C−C plane twists so as to give a torsional angle of at least 14.4°. The F-atoms at the C=C bond deviate from the C=C−C plane by at least 20.8°. As with c-$C_3F_4^-$, the optimized geometrical parameters depend very little on the different methods used, the bond lengths differing by no more than ≈0.1 Å and the bond angles by no more than ≈0.4°, except for variations of 2.2° in the C−C=C−C torsional angle and of 1.0° in the C−F bond deviation from the C=C−C plane.

The ^{19}F hf splittings computed for c-$C_4F_6^-$ are summarized in Table 3. The computations were carried out by four different methods, A, B, C and D. The electronic ground state of c-$C_4F_6^-$ is ^{2}A in a C_1 symmetry at all levels of theory. The computed splittings are well correlated with the experimental ones. Comparing the theoretical splittings with the experimental values definitive assignments of the three experimentally obtained triplet splittings of 15.2, 6.5, and 1.1 mT can be made, respectively, to the two fluorines (F9 & F10) at the C1=C2 carbons, the two fluorines (F5 & F7) at C3 and C4, and the other two fluorines (F6 & F8) at C3 and C4. Errors relative to the experimental isotropic ^{19}F hf splitting of c-$C_4F_6^-$ range from method D of 0.8% to method C of 3.3%, except for method B of 8.5% for the largest splitting. Figure 6c shows the SOMO projected to the $z-x$ plane, where the x-axis is parallel to the C3=C4 bond and the y-axis is parallel to the line connecting the centers of C1=C2 and C3−C4 bonds (see Inset 1). As with c-$C_3F_4^-$, the major part of the unpaired electron lies along the axes of the sp^3-like hybrid orbitals at the two olefin carbons. For reference purposes, the ^{19}F hf splittings computed for c-$C_4F_6^-$ with the geometry forced to the original planar C_s structure are also listed in Table 3a.

Octafluorocyclopentene: c-C5F8 and c-C5F8⁻. The molecular structure of c-C_5F_8 has been studied by gas phase electron diffraction.[50] The study revealed that the five-member carbon ring is a nonplanar C_s structure with the puckered angle of 21.9°;

TABLE 2: ESR Parameters Computed for *c*-$C_3F_4^-$

(a) ^{13}C and ^{19}F Hyperfine Splittings

state (symmetry)	exp[a]		^2A (C_2)	^2A (C_2)	^2A (C_2)	^2A (C_2)	$^2A_1$ (C_{2v})	$^2A_1$ (C_{2v})	$^2A_1$ (C_{2v})
ESR (method/basis sets)// geometry (method/basis sets):			A: B3LYP/6-311+G(2df,p)// B3LYP/6-311+G(d,p)	B: MP2/6-311+G(2df,p)// MP2/6-311+G(d,p)	C: B3LYP/6-311+G(2df,p)// MP2/6-311+G(d,p)	D: B3LYP/6-311+G(2df,p)// UHF/6-311+G(d)	A: B3L1YP/6-311+G(2df,p)// B3LYP/6-311+G(d,p)	B: MP2/6-311+G(2df,p)// MP2/6-311+G(d,p)	D: B3LYP/6-311+G(2df,p)// UHF/6-311+G(d)
^{13}C & ^{19}F hf splittings/mT		three ^{13}C							
		a (C1)	−0.66	−0.43	−0.58	−0.59	−0.14	2.07	−0.29
		a (C2 & C3)	6.61	5.24	6.40	5.78	1.11	5.29	−0.17
		two ^{19}F							
		a (F4 & F5)	−0.04	−0.44	−0.027	0.35	1.09	4.52	12.4
		B_{aa}	−0.63	−0.51	−0.62	−0.55			
		B_{bb}	0.25	0.13	0.24	0.18			
		B_{cc}	0.38	0.38	0.38	0.38			
	two ^{19}F atoms	two ^{19}F at F6 & F7 (C═C)							
	a: 18.4	a	18.1	17.4	18.3	17.4	52.84	62.9	39.9
	B_{aa}: −4.1	B_{aa}	−5.51	−4.49	−5.37	−5.08	−2.79	−6.02	−0.71
	B_{bb}: −4.1	B_{bb}	−4.39	−3.81	−4.30	−4.08	−2.68	−5.72	−0.66
	B_{cc}: 8.1	B_{cc}	9.90	8.30	9.67	9.16	5.47	11.74	1.37

(b) Direction Cosines for the Anisotropic ^{19}F Hyperfine Splittings and Isotropic Splittings[b]

^{19}F nucleus position[c]	^{19}F hf splitting in mT (direction cosines: *x*, *y*. *z* system)[c,d]
4 & 5	*a*: −0.03 B_{aa}: −0.62 (−0.2320, 0.2338, 0.9442) B_{bb}: 0.24 (0.9089, −0.2936, 0.2961) B_{cc}: 0.38 (0.3464, 0.9269, −0.1444)
6 & 7 (C═C)	*a*: 18.3 B_{aa}: −5.37 (−0.1257, 0.9323, 0.3391) B_{bb}: −4.30 (−0.2227, −0.3596, 0.9062) B_{cc}: 9.67 (0.9668, 0.0384, 0.2528)

[a] Reference 41. [b] Computed for the $^2A(C_2)$ state of *c*-$C_3F_4^-$ using method C. [c] See Figures 5 and 6 for the numbering of atoms and the *x*, *y*, *z* system. [d] The direction cosines for ^{19}F nucleus positions 5 and 7 are obtained by sign change of the *y* components.

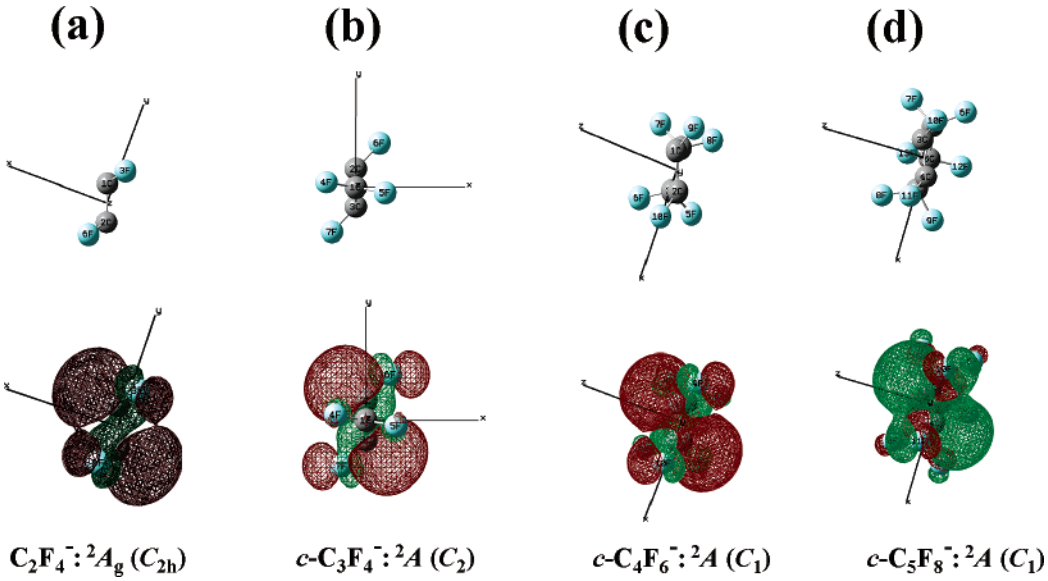

Figure 6. Singly occupied molecular orbitals (SOMOs) computed for $CF_2{=}CF_2^-$, c-$C_3F_4^-$, c-$C_4F_6^-$ and c-$C_5F_8^-$ with ground electronic states and point group symmetries (in parentheses). The computations were carried out using the B3LYP/6-311+G(2df,p)//UHF/6-31+G(d,p) method (method D).

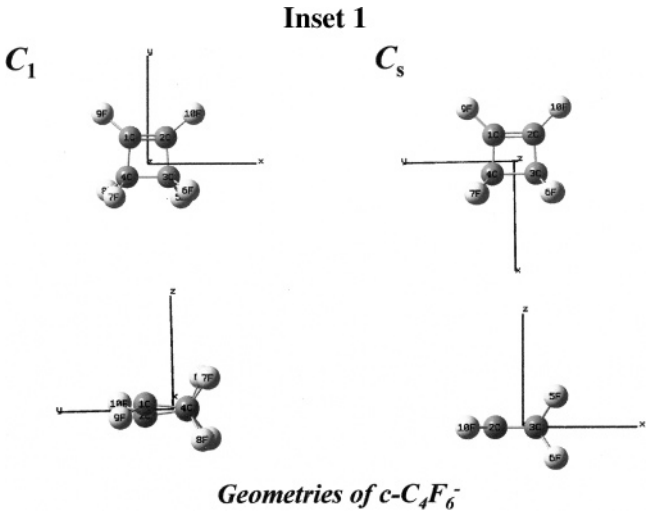

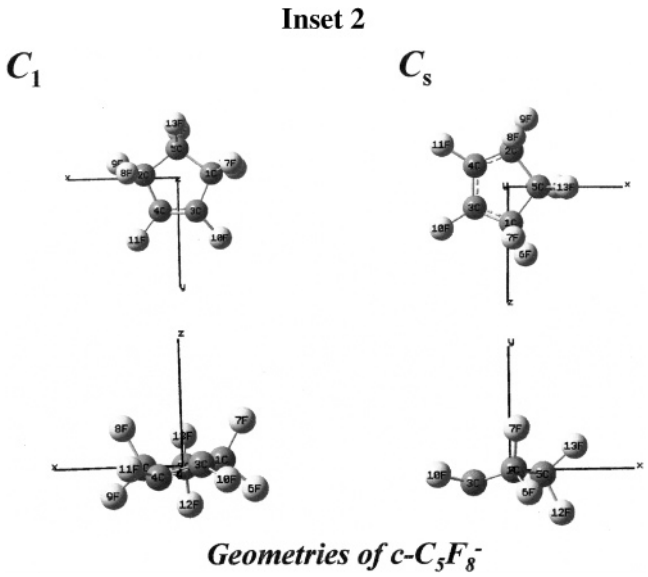

the expected ground electronic state is $^1A'$. The ^{19}F hf splittings of c-$C_5F_8^-$ were computed for two possible C_1 and C_s structures (see Inset 2). The results are summarized in Table 4.

The ^{19}F hf splittings computed for the C_s structure do not correspond well with the experimental ones. The computations for the twisted C_1 structure result in different splittings within each pair of fluorines (F10 & F11, F7 & F9 and F6 & F8), which is apparently inconsistent with the equivalent values obtained experimentally for each pair. However, the averaged splittings for each pair of fluorines are in reasonable agreement with the experimental ones at all levels of theory (Table 4). Thus, as with c-$C_4F_6^-$ we assign the three experimental triplet splittings of 14.7, 7.4 and 1.0 mT respectively to the two fluorines (F9 & F10) at the C3=C4 carbons, the two fluorines (F7 & F9) at C1 and C2, one at each carbon, and to the other two fluorines (F6 & F8) at C1 and C2; the attribution of the smallest splitting of 1.0 mT to another fluorine pair (F12 & F13) at C5 cannot be ruled out. To be consistent with the experimental results, ring inversion likely occurs at the higher matrix temperatures between the two enantiomeric C_1 structures of c-$C_5F_8^-$ on a time scale much faster than that corresponding to the small ^{19}F hf differences. Errors relative to the experimental isotropic splittings of c-$C_5F_8^-$ range from methods C and D of 6.0% to method B of 10.2% between method A of 7.2% for the largest splitting. Method D can give better overall agreement than method C as will be mentioned in the section of "Anisotropic ESR Spectra". Figure 6d shows the SOMO projected to the $z-x$ plane, where the x-axis is parallel to the line connecting C1 and C2 carbons and the y-axis is the line connecting the center of C3−C4 bond and C5 carbon (see Inset 2). As with c-$C_3F_4^-$ and c-$C_4F_6^-$ the majority of the unpaired electron lies again on the sp^3-like hybrid orbitals, suggesting a similar SOMO in these three perfluorocycloalkene radical anions.

Perfluoro-2-butene Anion: $CF_3CF{=}CFCF_3^-$. The neutral $CF_3CF{=}CFCF_3$ compound used in the present experiments consists of at least 97% *trans*-isomer and only 2% *cis*-isomer. The ^{19}F hyperfine splittings of $CF_3CF{=}CFCF_3^-$ were computed for the two possible cis- and trans-structures, both possessing C_2 symmetry, as shown in Figure 7. The computational results are summarized in Table 5.

It is difficult to unequivocally distinguish one structure from the other based on the small total energy difference of 4×10^{-3} eV. However, in the case of the large triplet splitting of 16.9

TABLE 3: ESR Parameters Computed for *c*-$C_4F_6^-$

(a) Isotropic ^{19}F Hyperfine Splittings

state (symmetry)	exp	^2A (C_1) twisted	^2A (C_1) twisted	^2A (C_1) twisted	^2A (C_1) twisted	$^2A''$ (C_s) coplanar
ESR (method/basis sets)// geometry (method/basis sets):		A: B3LYP/6-311+G(2df,p)// B3LYP/6-311+G(d,p)	B: MP2/6-311+G(d)// MP2/6-311+G(d)	C: B3LYP/6-311+G(2df,p)// MP2/6-311+G(d)	D: B3LYP/6-311+G(2df,p)// UHF/6-311+G(d,p)	A: B3LYP/6-311+G(2df,p)// B3LYP/6-311+G(d,p)
	three sets of two ^{19}F nuclei					
^{19}F isotropic hf splittings/mT	a_1(2F): 15.2	14.83 ± 0.03 (F9, F10)	13.87 ± 0.02 (F9, F10)	14.69 ± 0.11 (F9, F10)	15.07 (F9, F10)	5.11 (F5, F6, F7, F8)
	a_2(2F): 6.5	6.67 ± 0.02 (F5, F7)	5.40 ± 0.03 (F5, F7)	6.22 ± 0.02 (F5, F7)	6.32 (F5, F7)	2.24 (F9, F10)
	a_3(2F): (−)1.1	−1.49 ± 0.01 (F6, F8)	−2.07 ± 0.00 (F6, F8)	−1.63 ± 0.00 (F6, F8)	−1.50 (F6, F8)	

(b) Direction Cosines for the Anisotropic ^{19}F Hyperfine Splittings[a] and the Isotropic Splittings

^{19}F nucleus position[b]	^{19}F hf splitting in mT (direction cosines: *x*, *y*, *z* system)[c]
6 & 8	*a*: −1.50 B_{aa}: −0.54 (0.8689, −0.4563, 0.1916) B_{bb}: 0.08 (−0.0985, 0.2200, 0.9705) B_{cc}: 0.46 (0.4850, 0.8622, −0.1462)
5 & 7	*a*: 6.32 B_{aa}: −0.77 (0.8364, 0.2911, 0.4645) B_{bb}: −0.68 (−0.2884, −0.4869, 0.8245) B_{cc}: 1.45 (−0.4661, 0.8235, 0.3233)
9 & 10	*a*: 15.07 B_{aa}: −4.59 (−0.6223, 0.6836, 0.3814) B_{bb}: −3.69 (0.6807, 0.7132, −0.1674) B_{cc}: 8.28 (0.3865, −0.1554, 0.9091)

[a] Computed for the $^2A(C_1)$ state of *c*-$C_4F_6^-$ using method D. [b] See Figures 5 and 6 for the numbering of atoms and the *x*, *y*, *z* system. [c] The direction cosines for ^{19}F nucleus positions 8, 7 and 10 are obtained by sign change of the *y* components.

TABLE 4: ESR Parameters Computed for *c*-$C_5F_8^-$

(a) Isotropic ^{19}F Hyperfine Splittings

state (symmetry)	exp	^{2}A (C_1) twisted	^{2}A (C_1) twisted	^{2}A (C_1) twisted	^{2}A (C_1) twisted	^{2}A″ (C_s) nonplanar
ESR (method/basis sets)// geometry (method/basis sets):		A: B3LYP/6-311+G(2df,p)// B3LYP/6-311+G(d,p)	B: MP2/6-311+G(2df,p)// MP2/6-311+G(d,p)	C: B3LYP/6-311+G(2df,p)// MP2/6-311+G(d,p)	D: B3LYP/6-311+G(2df,p)// UHF/6-31+G(d,p)	A: B3LYP/6-311+G(2df,p)// B3LYP/6-311+G(d,p)
isotropic ^{19}F hf splittings/mT	a_1(2F): 14.7	13.5[a] (14.68, 12.29 for F10, F11)	13.2[a] (11.19, 15.26 for F10, F11)	13.7[a] (11.70, 15.60 for F10, F11)	13.6[a] (13.34, 13.81 for F10, F11)	7.49 (F7, F8)
	a_2(2F): 7.4	8.6 (10.21, 7.05 for F7, F9)	7.1 (9.34, 4.83 for F7, F9)	8.1 (10.50, 5.77 for F7, F9)	6.6 (7.32, 5.79 for F7, F9)	4.36 (F10, F11)
	a_3(2F): 1.0	0.9 (1.54, 0.33 for F12, F13)	0.8 (0.36, 1.26 for F12, F13)	0.9 (−0.02, 1.89 for F12, F13)	0.8 (0.60, 0.90 for F12, F13)	3.90 (F6, F9)
		−0.5 (−0.52, −0.50 for F6, F8)	−0.9 (−0.66, −1.06 for F6, F8)	−0.7 (−0.57, −0.89 for F6, F8)	−0.7 (−0.65, −0.80 for F6, F8)	−0.89, −0.19 (F12, F13)

(b) Direction Cosines for the Anisotropic ^{19}F Hyperfine Splittings[c] and the Isotropic Splittings

^{19}F nucleus position[d]	^{19}F hf splitting in mT (direction cosines: *x*, *y*. *z* system)[d]
6F	*a*: −0.65
	B_{aa}: −0.50 (0.7527, −0.6583, −0.0038)
	B_{bb}: −0.28 (−0.1876, −0.2201, 0.9573)
	B_{cc}: 0.78 (0.6310, 0.7198, 0.2892)
7F	*a*: 7.32
	B_{aa}: −0.10 (0.4053, −0.0531, 0.9126)
	B_{bb}: −1.02 (−0.5642, 0.7710, 0.2954)
	B_{cc}: 2.06 (0.7194, 0.6346, −0.2825)
8F	*a*: −0.80
	B_{aa}: −0.61 (0.8305, 0.5568, −0.0150)
	B_{bb}: −0.40 (−0.3537, 0.5481, 0.7579)
	B_{cc}: 1.01 (0.4303, −0.6241, 0.6522)
9F	*a*: 5.79
	B_{aa}: −0.85 (0.0865, 0.0965, 0.9916)
	B_{bb}: −0.84 (0.5701, 0.8114, −0.1288)
	B_{cc}: 1.69 (0.8170, −0.5765, −0.0152)
10F	*a*: 13.34
	B_{aa}: −4.40 (−0.4681, 0.8240, 0.3193)
	B_{bb}: −3.54 (0.8054, 0.5464, −0.2296)
	B_{cc}: 7.94 (0.3636, −0.1497, 0.9194)
11F	*a*: 13.81
	B_{aa}: −4.26 (0.4521, 0.7999, −0.3948)
	B_{bb}: −3.43 (0.8100, −0.5535, −0.1938)
	B_{cc}: 7.69 (0.3735, 0.2322, 0.8981)

[a] Average values of the two ^{19}F hf splittings. [b] Some geometrical parameters computed by method D. $l_{C=C}$ = 1.416 Å, the C═C−F bond angle: 119.2°. Dihedral angle of the C−F bond with the C═C−C plane: 25.1°. F−C═C−F torsional angle: 61.9°. [c] Computed for the $^2A(C_1)$ state of *c*-$C_5F_8^-$ using method D. [d] See Figures 5 and 6 for the *x*, *y*, *z* system.

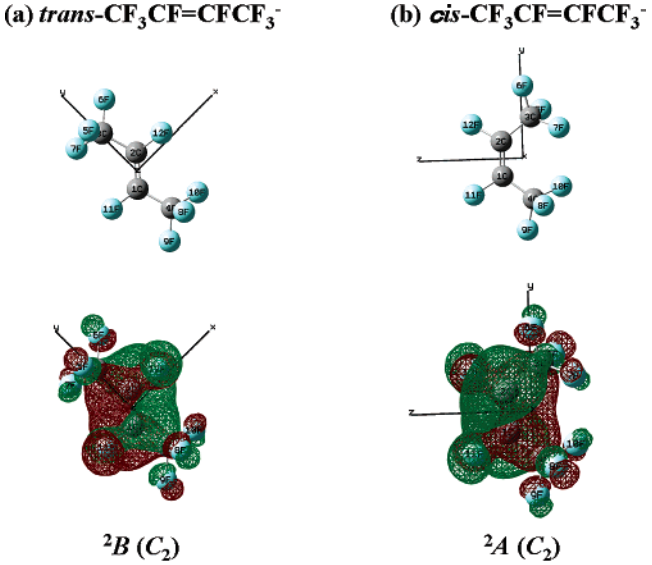

Figure 7. Geometrical structures and SOMOs computed for *trans*-$CF_3CF{=}CFCF_3^-$ and *cis*-$CF_3CF{=}CFCF_3^-$ with ground electronic states and point group symmetries (in parentheses). The computations were carried out using the B3LYP/6-311+G(2df,p)//UHF/6-31+G(d,p) method (method D).

mT, the computational results for the trans-structure are in better agreement than the results calculated for the cis-structure. This may indicate that the original trans-geometrical form of CF_3-$CF{=}CFCF_3$ is preserved after one-electron reduction. The computations support the assignment of the large triplet to two equivalent "α"-fluorines attached to the C1=C2 bond. Furthermore, the average of the three different splittings computed for the CF_3 fluorines agrees reasonably well with the experimental value; this is consistent with free rotation of the CF_3 group about the C2−C3 (and C1−C4) bond. Plots of the computed SOMO are illustrated together with the *cis*- and *trans*-structures in Figure 7. It is clearly seen that the majority of the unpaired electron again lies along the axes of the sp^3-like hybrid carbon orbitals.

Tetrafluoroethylene Anion: $CF_2{=}CF_2^-$. Paddon-Row et al. have computed the geometries of the radical anions of $CH_2{=}CH_2^-$, $CH_2{=}CHF^-$, $CH_2{=}CF_2^-$ and $CF_2{=}CF_2^-$ using the ab initio UHF method with the 3-21G basis set.[13] They reported that the planar structures are not stable minima for all four radical anions, and that upon optimization the planar structures relax to the anti-bent structures. The degree of pyramidalization at the carbons in these radical anions increases with fluorine substitution, paralleling the well-known effect for fluorinated methyl radicals.[26−31] Fluorine is well-known for its weak π-donating and very strong σ-inducing effect. Thus the introduction of fluorine atoms into $CH_2{=}CH_2$ significantly affects the relative energy of the π- and σ-levels[51] and thus the out-of-plane distortions. Recently, Hou and Huang[18] have confirmed the anti-bent structure of $CH_2{=}CF_2^-$ and $CF_2{=}CF_2^-$ by using ab initio methods with large basis sets, and reported that their isotropic ^{19}F hf splittings computed using the B3LYP and MP2-(full) methods with the 6-311+G(d,p) basis set are in good agreement with experiment. However, the anisotropic ^{19}F hf splittings of $CF_2{=}CF_2^-$ computed by the ab initio methods are not available in the literature. Therefore, in addition to confirming the reported anti-bent structural distortion using the B3LYP, MP2 and UHF methods with the 6-311+G(d,p) basis set, we have computed both the isotropic and anisotropic ^{19}F and ^{13}C hf splittings of $CF_2{=}CF_2^-$ to compare these values with the corresponding results for the perfluorocycloalkene radical anions.

The computational results obtained by the four different methods, A, B, C and D are summarized in Table 6. The electronic ground state of $CF_2{=}CF_2^-$ is ^2A_g in the anti-bent C_{2h} structure at all levels of theory. The computed splittings are well correlated with the experimental ones, especially for the isotropic ^{19}F splitting. Errors relative to the experimental isotropic ^{19}F hf splitting of $C_2F_4^-$ range from method A of 1.5% to method B of 6.2%, with intermediate errors of 2.3% and 2.9% for methods D and C, respectively. The agreement in the isotropic ^{13}C splitting is slightly less satisfactory than that in the ^{19}F hf splitting, (see Table 6). In summary, the strong distortions in $CF_2{=}CF_2^-$ originate from a mixing of the π^* and the higher-lying σ^* orbitals at the C=C bond, the situation being similar to that for the acetylene anion whose structure is also distorted due to the $\sigma^*-\pi^*$ mixing.[52−55] The present work makes it clear that the structural distortion in the perfluorocycloalkene radical anions can also be primarily attributed to a similar effect occurring at the C=C carbons. The anisotropic ^{19}F hf splittings will be discussed together with the anisotropic ESR spectra in a later section.

3.3. Anisotropic ESR Spectra: Experimental Results vs Computations.

c-$C_3F_4^-$. The present computations predict that the c-$C_3F_4^-$ radical anion has a ^{2}A electronic ground state (in C_2 symmetry) with two sets of two magnetically equivalent ^{19}F nuclei as summarized in Table 2a. The computed ^{19}F hf splittings reproduce quite well the isotropic experimental values.[41] The theoretical splittings giving the best fit are obtained by computations using the B3LYP method (with 6-311+G(2df,p) basis set) with the geometry optimized by the MP2 method (with 6-311+G(d,p) basis set). Although the experimental anisotropic ESR spectrum of c-$C_3F_4^-$ has not been reported, it is of interest to theoretically predict the spectrum. Using ^{19}F hf splittings and the direction cosines obtained by method C giving the best fit (see Table 2b), the computed ESR spectrum is shown in Figure 8 and is characteristic of two magnetically equivalent ^{19}F atoms with axially symmetric hf splittings. Specifically, the B3LYP computations resulted in the two ^{19}F-atoms at the C=C bond (F6 and F7) having large anisotropic hf splittings close to axial symmetry that dominate the ESR spectrum. The hf splittings due to the other two ^{19}F-atoms at C1 (F4 and F5) are within the line width used (0.7 mT) and consequently are too small to be resolved in the simulated ESR spectrum. The $x-y$ projection of the SOMO in Figure 6b points to the principal directions of the maximum splittings of B_{cc} at F6 and F7. The angles calculated from the direction cosines in Table 2b are (+15°, +88° and +75°) and (+15°, −88° and +75°) from the x, y and z axis, respectively; the SOMOs at F6 and F7 lie almost in the $z-x$ plane and in a C_2 symmetry with respect to an axis perpendicular to the y axis which is parallel to the C2=C3 bond. Judging from the good agreement in c-$C_4F_6^-$ and c-$C_5F_8^-$ spectra, which will be mentioned in the following sections, the computed anisotropic ESR spectrum of c-$C_3F_4^-$ is expected to fit very closely to the experimental one and therefore its future observation would be of interest.

c-$C_4F_6^-$. Figure 2a shows an anisotropic spectrum of c-$C_4F_6^-$ in TMS-d_{12} recorded at 90 K. The spectral line shape is quite complicated with a number of anisotropic hf lines due to three different pairs of ^{19}F nuclei. It is very difficult to analyze the experimental "powder" spectrum and evaluate the ^{19}F hf tensors on the basis of the ordinary trial method for ESR spectral

TABLE 5: Isotropic ^{19}F Hyperfine Splittings Computed for $CF_3CF{=}CFCF_3^-$

	exp	trans structure	trans structure	cis structure	cis structure
state (symmetry)		^2B (C_2)	^2B (C_2)	^2A (C_2)	^2A (C_2)
ESR (method/basis sets)// geometry (method/basis sets)		A: B3LYP/6-311+G(2df,p)// B3LYP/6-311+G(d,p)	D: B3LYP/6-311+G(2df,p)// UHF/6-311+G(d,p)	A: B3LYP/6-311+G(2df,p)// B3LYP/6-311+G(d,p)	D: B3LYP/6-311+G(2df,p)// UHF/6-311+G(d,p)
isotropic ^{19}F hf splittings	two equivalent ^{19}F nuclei				
	a_1(2F): 16.93	14.85 (F11 & F12)	15.98 (F11 & F12)	13.2 (F11 & F12)	12.02 (F11 & F12)
	six equivalent ^{19}F nuclei				
	a_2(6F): 2.56	2.52[a] [4.98 (2F), 2.66 (2F), −0.09 (2F)]	1.95[a] [2.54 (2F), 3.57 (2F), −0.23 (2F)]	3.10[a] [2.61 (2F), 6.93 (2F), −0.23 (2F)]	1.79[a] [2.024 (2F), 3.500 (2F), −0.169 (2F)]

[a] Average values of six ^{19}F hf splittings belonging to two CF_3 groups.

TABLE 6: ESR Parameters Computed for $CF_2{=}CF_2^-$

(a) Isotropic ^{13}C and ^{19}F Hyperfine Splittings

state (symmetry)	exp[a]	^2A_g (C_{2h})	^2A_g (C_{2h})	^2A_g (C_{2h})	^2A_g (C_{2h})
ESR (method/basis sets)// geometry (method/basis sets)		A: B3LYP/6-311+G(2df,p)// B3LYP/6-311+G(d,p)	B: MP2/6-311+G(2df,p)//MP2// 6-311+G(d,p)	C: B3LYP/6-311+G(2df,p)// MP2//6-311+G(d,p)	D: B3LYP/6-311+G(2df,p)// UHF/6-311+G(d)
^{13}C	a: 4.87	5.17	4.37	4.99	4.29
(two equivalent)	B_{aa}:	−1.63	−1.54	−1.62	−1.59
hf splitting/mT	B_{bb}:	−1.45	−1.39	−1.44	−1.42
	B_{cc}:	3.08	2.93	3.05	3.01
^{19}F	a: 9.49	9.63	8.90	9.77	9.71
(four equivalent)	B_{aa}: −2.05	−2.93	−2.55	−2.90	−2.78
hf splitting/mT	B_{bb}: −2.05	−2.41	−2.10	−2.39	−2.37
	B_{cc}: 4.1	5.34	4.64	5.29	5.15

(b) Direction Cosines for the Anisotropic ^{19}F Hyperfine Splittings[b] and the Isotropic Splitting

	^{19}F hf splitting in mT (direction cosines: x, y, z)[c,d]
^{19}F (four equivalent)	a: 9.71 B_{aa}: −2.78 (0.2423, 0.2479, 0.9380) B_{bb}: −2.37 (−0.1975, 0.9592, −0.2025) B_{cc}: 5.15 (0.9499, 0.1362, −0.2814)

[a] Reference 10. [b] Computed for the $^2A(C_1)$ state of $CF_2{=}CF_2^-$ using method D. [c] See Figures 5 and 6 for the x, y, z system. [d] Direction cosines for one of the four ^{19}F. The other direction cosines are obtained by assuming C_{2h} symmetry for the $C_2F_4^-$ anion.

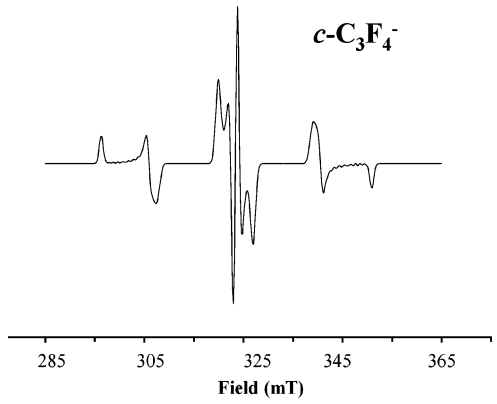

Figure 8. Theoretical anisotropic ESR spectrum of c-$C_3F_4^-$. The computations were carried out using the principal values and principal directions of ^{19}F ($I = {}^1/_2$) hf splittings by the B3LYP/6-311+G(2df,p)// MP2/6-31+G(d,p) method (method C) given in Table 2b. In the spectral computations a constant Gaussian line width of 0.7 mT was used.

simulation because of the large number of adjustable parameters; one not only needs to consider the ^{19}F hf principal values (3 parameters), but also their directions (3 parameters) should be considered for each of the six ^{19}F nuclei. On the other hand, as mentioned above, the experimental isotropic ^{19}F hf splittings are reproduced with very high accuracy by method D, i.e., the DFT [B3LYP/6-311+G(2df,p)] computations for the C_1 geometry optimized by the UHF/6-311+G(d,p) method; $a_1 = 15.2$ (exp) vs 15.07 (cal) mT for two ^{19}F nuclei, $a_2 = 6.5$ (exp) vs 6.32 (cal) mT for two ^{19}F, $a_3 = (-)1.1$ (exp) vs −1.50 (cal) mT for two ^{19}F nuclei; see Table 3a. This good agreement in the isotropic ^{19}F hf splittings encouraged us to compute an anisotropic "powder" spectrum of c-$C_4F_6^-$ using the computed principal values and directions of ^{19}F nuclei; the ^{19}F hyperfine tensors used for the spectral computations are given in Table 3b. The computed ESR spectrum is compared with the experimental one in Figure 9. The overall spectral features are reproduced quite well although the detailed line positions and relative intensities are not in perfect agreement with the experimental ones; the line positions and intensities depend rather sensitively on both the ^{19}F principal values and directions, and further spectral improvement would require large computation time and efforts to optimize those parameters. In particular, the outermost anisotropic doublet with a small triplet substructure of 1.1 mT is well reproduced in the computed spectrum. The total ^{19}F hf spectral width between the calculated outermost

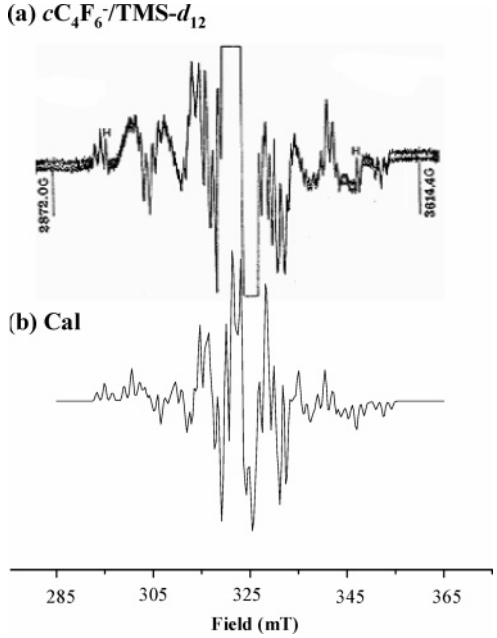

Figure 9. (a) ESR spectrum of c-$C_4F_6^-$ in TMS-d_{12} at 90 K (ν = 9121.4 Hz). (b) Theoretical ESR spectrum of c-$C_4F_6^-$ computed using the principal values and principal directions of ^{19}F ($I = {}^1/_2$) hf splittings by the B3LYP/6-311+G(2df,p)//UHF/6-31+G(d,p) method (method D) given in Table 3b. In the spectral computations a constant Gaussian line width of 1.68 mT was used.

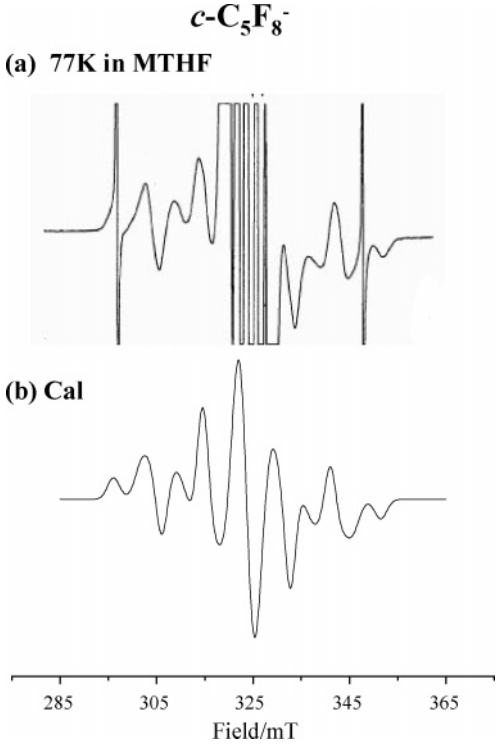

Figure 10. (a) First derivative ESR spectrum of c-$C_5F_8^-$ in MTHF at 77 K. (b) ESR spectrum of c-$C_5F_8^-$ computed using the principal values and principal directions of ^{19}F ($I = {}^1/_2$) hf splittings by the B3LYP/6-311+G(2df,p)//UHF/6-31+G(d,p) method (method D) given in Table 4b. In the spectral computations a constant Gaussian line width of 1.4 mT was used.

doublet (defined by the central lines of the small triplet substructure of the outermost doublet) is 57.3 mT, which is only 0.6 mT larger than the experimental width (56.7 mT); the error with respect to the experimental total splitting is therefore only 1.0% and it may be said that the spectral agreement is surprisingly good. We also note here that, consistent with these arguments, no appreciable spectral improvement was obtained when the anisotropic spectrum was computed using the experimentally observed isotropic hf splittings and the computed hf anisotropy (method D). Thus, we conclude that the computed anisotropic ^{19}F hf tensors (the principal values of the splittings and their orientation) are quite close to the experimental ones, similar to the good agreement found for the isotropic ^{19}F hf splittings.

The present computations predict that the c-$C_4F_6^-$ radical possesses a ^2A electronic ground state (in C_1 symmetry) in which the six ^{19}F nuclei are grouped into three sets of two magnetically equivalent ^{19}F nuclei, as summarized in Table 3b. The two ^{19}F-atoms at the F9 and F10 positions attached to the C=C bond give the largest anisotropic (as well as the isotropic) hf splittings, which therefore predominate in the ESR anisotropic pattern. The anisotropic hf splittings correspond closely to axial symmetry: (B_{aa}, B_{bb}, B_{cc}) = (−45.9, −36.9, +82.8 mT). The principal direction of B_{cc}, which corresponds to the maximum splitting, should occur along the orientation suggested by the shape of the SOMO for c-$C_4F_6^-$. In fact, the $z-x$ projection in Figure 5c shows the SOMO at F9 and F10 to point to the principal directions of B_{cc} given in the table. The angles calculated from the direction cosines are 67°, ±81° and 24° from the x, y and z axis; the orientation of B_{cc} at F9 and F10 being in a C_2 symmetry with respect to an axis perpendicular to the y-axis, which is the line connecting the centers of the C1=C2 and C3−C4 bonds.

c-$C_5F_8^-$. The computations predict a c-$C_5F_8^-$ radical anion possessing a ^2A (in C_1 symmetry) ground state as summarized in Table 4a. The best fit for the isotropic ^{19}F splittings are obtained by the computations using either method C or D. Figure 10a shows an anisotropic spectrum of c-$C_5F_8^-$ generated in irradiated MTHF matrix and recorded at 77 K. The central part of the spectrum is overlapped with a strong quintet from a matrix radical. The eight broad anisotropic features present in both wings are attributable to c-$C_5F_8^-$. An anisotropic spectrum was computed using the ^{19}F hf splittings and the direction cosines obtained by method D (see Table 4b). The computed spectrum agrees quite well with the experimental one, as shown in Figure 10. The spectral line shape is essentially determined by the four ^{19}F nuclei with the larger hf splittings; the remaining four ^{19}F nuclei with the smaller hf splittings contribute negligibly to the line shape because of the large Gaussian line width of 1.4 mT observed experimentally and used for the simulations. The anisotropic ^{19}F hf splittings of c-$C_5F_8^-$ are rather close to those of c-$C_4F_6^-$, as is the case with the isotropic ones (see Tables 1, 3 and 5), reflecting a close similarity in their local electronic structure around the C=C bond. Consistent with this, the anisotropic ESR line shapes for both radical anions resemble each other, except for the large spectral line width in c-$C_5F_8^-$, which smears out the smallest triplet splitting of ca. 1 mT in the spectrum.

We also computed the anisotropic spectrum using the ^{19}F hf splittings and the direction cosines obtained by method C. However, the computed spectrum resulted in worse agreement with the experimental spectrum (the computed spectrum is not shown here). Method C resulted in rather different hf splittings for the F7 and F9 pair having the largest splittings, as can be seen in Table 4a. This may be the reason for the worse fit to the experimental spectrum.

CF_2=CF_2^-. As previously reported by two of the present authors,[10] the rigid-limit ESR spectrum of CF_2=CF_2^- in the MTHF matrix can be formally analyzed in terms of the parallel and perpendicular components of axially symmetric hyperfine

tensors from four magnetically equivalent ^{19}F atoms; $A_{||}(4F) = 13.59$ and $A_{\perp}(4F) = 7.44$ mT. Assuming that these principal values have the same sign, the derived isotropic ^{19}F hf splitting, $a(4F) = 9.49$ mT, is in excellent agreement with the value of 9.43 mT obtained directly from the isotropic spectrum measured in TMS-d_{12}.[10,11] Moreover, these experimental results for the isotropic splitting are in accord with the average value of $a(4F) = 9.50$ mT computed by the theoretical methods A−D listed in Table 6a for the ^2A_g ground state of the $CF_2{=}CF_2^-$ radical anion with an anti-bent C_{2h} chair structure.

Turning now to the anisotropic tensor components, a similar concordance between experiment and theory is not expected because the direction cosines of the four fluorines for this C_{2h} chair structure are only equivalent in the fluorine pairs, (F3 & F5) and (F4 & F6), that are related through the inversion operation. Indeed, according to the geometry of the C_{2h} structure, it can be anticipated that the reported axially symmetric ^{19}F hf splittings may only actually be "effective" ones, i.e., values resulting from projection to a common axis for all four fluorines. Consequently, the "true" anisotropic hf values may be significantly larger than the experimentally reported ones. In fact, the computed anisotropic ^{19}F splittings are larger by 15−36% than the reported ones: (exp: −2.05, −2.05, +4.1 mT) vs (cal: −2.78, −2.37, +5.15 mT). This difference is reminiscent of similar observations for the randomly oriented trifluoromethyl ($CF_3^{\bullet}$) radical,[29−31] where a measured coupling of 25.22 mT was identified with the component along the 3-fold symmetry axis of an effective tensor, whereas the true hyperfine coupling tensor of the three ^{19}F nuclei had principal values of 8.7, 8.0 and 26.35 mT.[29,30] Similarly, the effect of nonparallel principal axes for $CF_2{=}CF_2^-$ is likely to cause the magnitude of the largest principal value of the ^{19}F tensor, and hence the anisotropy, to be underestimated experimentally.

The theoretical powder spectrum of $CF_2{=}CF_2^-$ was then computed using the isotropic and anisotropic ^{19}F splittings and their direction cosines calculated by method D, as listed in Table 6b. As shown in Figure 11, the computed spectral features correspond quite well with the experimental ones. Furthermore, the total spectral width of 57.2 mT only exceeds the experimental value of 54.4 mT (4 × 13.59 mT) by 5%. Thus, as with the perfluorocycloalkene radical anions, the present computations by method D indicate that the calculated ^{19}F hf tensors must be very close to the "true" ones.

Considering now the apparent equivalence of the four fluorines as revealed by the prominent "parallel" and "perpendicular" features in both the experimental and computed powder spectra, it is seen that the $x-y$ projection of the SOMO in Figure 6a points to the principal directions of the maximum splitting (B_{cc}) for F3 (& F5) and F4 (& F6). In agreement with this figure and the direction cosines in Table 6b, these nuclei become equivalent in the $x-y$ plane and along the z axis, which is a C_2 symmetry axis with regard to the ^{19}F hf tensors. The maximum ^{19}F hf splitting in the $x-y$ plane was evaluated with standard formulas[56] from the data in Table 6b to be 14.4 mT, which predicts an overall width between the outermost "parallel" features of 57.6 mT (14.4 mT x 4), in close agreement with the value of 57.2 mT measured from the computed spectrum in Figure 11.

The maximum (or parallel) hf splitting of 13.6 mT obtained from the previous analysis[10] of the anisotropic spectrum of $CF_2{=}CF_2^-$ in the MTHF matrix can accordingly be thought of as an "effective" parallel value corresponding to the maximum splitting in the $x-y$ plane. Similarly, the calculated minimum in this plane and the component along the z axis (7.3 and 6.9 mT, respectively) can be identified with an "effective" perpendicular coupling of 7.4 mT in the experimental spectrum. To summarize, the observed B_{cc} of 4.1 mT (13.6−9.5 mT) agrees reasonably well with the calculated "effective" anisotropic splitting B_{cc} of 4.7 mT (14.4−9.7 mT; see method D in Table 6a). According to this analysis, however, the effect of nonparallel principal axes causes the latter to be smaller by 9% than the "true" theoretical value of 5.15 mT.

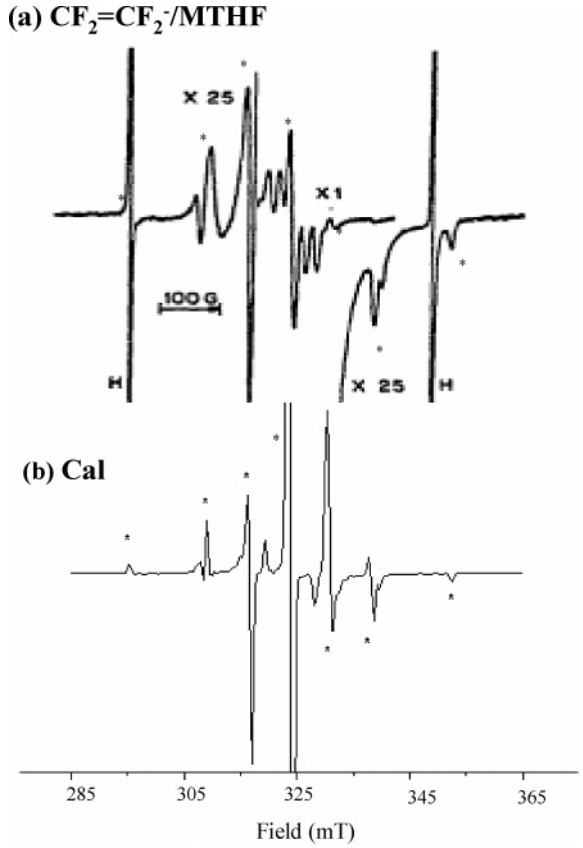

Figure 11. (a) ESR spectra of a γ-irradiated solid solution of 1 mol % $CF_2{=}CF_2$ in MTHF recorded at 83 K [adapted from ref 10]. The signals indicated by * are due to $CF_2{=}CF_2^-$. (b) ESR spectrum of $CF_2{=}CF_2^-$ computed using the principal values and principal directions of ^{19}F ($I = {}^1/_2$) hf splittings by the B3LYP/6-311+G(2df,p)//UHF/6-31+G(d,p) method (method D) given in Table 6b. In the spectral computations a constant Gaussian line width of 0.6 mT was used.

Finally, it is of interest to compare the ^{19}F hf splitting of $CF_2{=}CF_2^-$ with the values for the corresponding "α"-fluorines of c-$C_3F_4^-$. Both the isotropic and anisotropic ^{19}F hf splittings of c-$C_3F_4^-$ are about twice as large as those of $CF_2{=}CF_2^-$, the experimental splittings being $a_{iso} = +18.4$ and $B_{cc} = +8.2$ mT for c-$C_3F_4^-$ and $a_{iso} = +9.5$ and $B_{cc} = +4.1$ mT for $CF_2{=}CF_2^-$ (Tables 1, 2 and 6). This can be rationalized as follows: the c-$C_3F_4^-$ anion has two "α"-fluorines with respect to the C=C bond, whereas the $CF_2{=}CF_2^-$ has four "α"-fluorine atoms. The SOMO consists formally of an sp^3-like hybrid orbital in a pyramidal structure resulting from the mixing of the π^* and higher-lying σ^* at the C=C bond, as mentioned above. Assuming that both anions have the same total spin density in the hybrid orbital, and that the total extent of delocalization into the "α"-fluorine orbitals is independent of the number of "α"-fluorines, the shared spin density in each of the "α"-fluorine orbitals then becomes inversely proportional to the number of attached "α"-fluorines, consistent with observation.

3.4. Electronic Spectra. Electronic excitation energies and oscillator strengths were computed for $CF_2{=}CF_2^-$, c-$C_3F_4^-$, c-$C_4F_6^-$ and c-$C_5F_8^-$ radical anions. In Figure 12 their oscillator

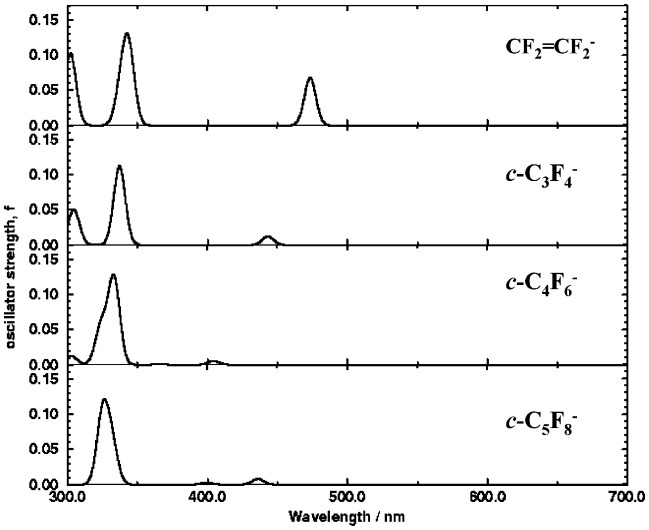

Figure 12. (a) Electronic absorption spectra of CF_2=CF_2^-, *c*-$C_3F_4^-$, *c*-$C_4F_6^-$ and *c*-$C_5F_8^-$ computed by DT (time-dependent) B3LYP DFT method (6-311+G (d,p) basis set). The oscillator strengths (*f*) are plotted in 300−700 nm (UV−visible light) range. See text for details.

strengths (*f*) are plotted in the 300−700 nm range (UV−visible light range); for the numerical values refer to Supporting Information 3. Weak absorption lines with $f = 0.06-0.07$ are predicted in the visible range of 400−700 nm; $\lambda_{max} = 473$, 443, 404 and 436 nm for CF_2=CF_2^-, *c*-$C_3F_4^-$, *c*-$C_4F_6^-$ and *c*-$C_5F_8^-$, respectively. For the former three radical anions, the lowest excitation energies can be mainly attributed to the electron transitions at the C=C bond with 24B → 25B, 27B → 28B and 39B → 40B. It may be of interest to point out that an increase in molecular size from *n* (number of carbons) = 2 to *n* = 4 results in a "blue" shift with decreasing oscillator strengths. The prediction of light absorption in the visible region is consistent with the present experimental results showing that all the ESR spectral lines attributable to the radical anions are removed by exposure of the sample to unfiltered light from a tungsten lamp. A suggested reaction is a simple photoelectron detachment from the radical anions.[57] In fact, we have previously observed that electrons can be transferred from a perfluorocycloalkane radical anion to SF_6 (with a larger electron affinity) by photobleaching when the latter is incorporated in the matrix.[8] Experimental electronic spectra of the perfluoroalkene radical anions are not available in the literature. Thus the present computations provide useful information about the excitation energies and oscillator strengths of these fundamentally important chemical species.

4. Concluding Remarks

The radical anions of hexafluorocyclobutene (*c*-$C_4F_6^-$), octafluorocyclopentene (*c*-$C_5F_8^-$) and perfluoro-2-butene (CF_3CF=$CFCF_3^-$) were generated by electron attachment to the solute in a γ-irradiated solid matrix at 77 K and subjected to an ESR study. The "isotropic" spectra were observed using plastically crystalline neopentane, tetramethylsilane (TMS) and TMS-d_{12} as matrix molecules.[7,8,10,11] The spectra of *c*-$C_4F_6^-$ and *c*-$C_5F_8^-$ are characterized by three different sets of pairs of ^{19}F nuclei with the following isotropic hf splittings: 15.2 (2F), 6.5 (2F), 1.1 (2F) mT for *c*-$C_4F_6^-$ and 14.7 (2F), 7.4 (2F), 1.0 (2F) mT for *c*-$C_5F_8^-$. The isotropic ESR spectrum of CF_3CF=$CFCF_3^-$ was also observed in a TMS matrix with a triple septet with 16.9 (2F) and 2.6 (6F) mT splittings. Other simple perfluoroalkene radical anions, whose isotropic ^{19}F hf splittings are available, are *c*-$C_3F_4^-$ [41] and CF_2=CF_2^- [10,11] with 18.9 (2F) mT and 9.43 (4F) mT, respectively.

By comparison with the results of ab initio quantum chemical computations, the large ^{19}F hf splittings of 9−19 mT observed for the perfluoroalkene radical anions are attributable to the two ^{19}F nuclei attached to the C=C bond. The UHF, B3LYP and MP2 computations all predict a structural distortion of the perfluoroalkenes after a one-electron reduction to form their radical anions; *c*-$C_3F_4^-$, C_2 symmetry (^{2}A electronic ground state) ← C_{2v} (^{1}A$_1$); *c*-$C_4F_6^-$, C_1 (^{2}A) ← C_{2v} (^{1}A$_1$); *c*-$C_5F_8^-$, C_1 (^{2}A) ← C_s (^{1}A′). The structural distortion arises from a mixing of the π^* and higher-lying σ^* orbitals so as to give a pyramidal structure at the C=C carbons similar to that for unsaturated alkyne and alkene radical anions such as the acetylene[52−55] and ethylene radical anions,[13] including those with fluorine substitutions. In each case the unpaired electron is primarily localized in the sp^3-like hybrid orbitals formed by the π^* and σ^* orbital mixing and is transferred to the fluorine orbitals so as to give large hf splittings for the two ^{19}F nuclei at the original C=C bond. Consistent with this argument, a close similarity is found for the SOMOs of $C_2F_4^-$, *c*-$C_3F_4^-$, *c*-$C_4F_6^-$ and *c*-$C_5F_8^-$ (see Figure 6). It may be of interest to point out here that the isotropic hf splittings to the two "β"-fluorines (F4 and F5 in Table 2) in *c*-$C_3F_4^-$ are so small relative to those for the "β"-fluorines (a_2(2F) = 6.5 mT) in *c*-$C_4F_6^-$. The much smaller "β"-fluorine couplings in *c*-$C_3F_4^-$ may well be related to the fact that in this case, these "β"-fluorine atoms F4 and F5 lie in a plane which corresponds to a largely nodal region of the SOMO, depicted in Figure 6b, whereas this special geometrical situation does not apply for the "β"-fluorines in *c*-$C_4F_6^-$. The isotropic ^{19}F hf splittings computed with the B3LYP method with 6-311+G-(2df,p) basis set for the geometry optimized by the UHF and/or MP2 methods are within 6% error of the experimental values. Considering the large value of the atomic hyperfine constant[58] for ^{19}F and its high sensitivity to the structural distortions, this agreement in the isotropic splittings is extremely gratifying.

The anisotropic ^{19}F hf splittings can potentially provide more detailed experimental information about the electronic structure of the radical anions. Thus we observed fully anisotropic ESR spectra of *c*-$C_4F_6^-$ in TMS-d_{12} and *c*-$C_5F_8^-$ in MTHF at low temperatures close to 77 K. At first we thought that it would be very difficult to analyze the experimental "powder" spectrum using an ordinary ESR spectral simulation method because of the large number of adjustable parameters which include ^{19}F hf principal values (3 parameters) and their directions (3 parameters). However, the excellent agreement between the theoretical isotropic ^{19}F hf splittings and the experimental ones encouraged us to calculate the anisotropic "powder" spectra using the computed hf principal values and the orientation of the ^{19}F hf tensors. Finally, the experimental anisotropic spectra of *c*-$C_4F_6^-$ and *c*-$C_5F_8^-$ were satisfactorily reproduced by the ESR spectral simulation method using the computational results, especially the C {B3LYP/6-311+G(2df,p)//MP2/6-311+G(d,p)} or D {B3LYP/6-311+G(2df,p)//UHF/6-311+G(d,p)} methods. Furthermore, we note that the two radical anions have the ^{19}F hf structures close to each other, reflecting a close similarity in the local electronic structure about the C=C bond.

In the same manner the rigid-limit anisotropic ESR spectrum of CF_2=CF_2^- was also satisfactorily simulated using the computational results. Thus, it is concluded that, in addition to the isotropic ^{19}F hyperfine splittings, the anisotropic ^{19}F hf splittings can be quite well predicted by the computations using the B3LYP, MP2 and UHF methods with 6-311+G(2df,p) basis set for the radical anions of simple perfluoro cycloalkenes and linear alkenes. We also computed an anisotropic spectrum of *c*-$C_3F_4^-$, the simplest perfluorocycloalkene radical anion, al-

though the experimental spectrum has not yet been reported. Both the isotropic and anisotropic ^{19}F hf splittings of *c*-$C_3F_4^-$ are about twice as large as those of $C_2F_4^-$. This suggests that both anions have almost the same kind of hybrid orbital for the unpaired electron, but that the degree of unpaired electron delocalization to the "α"-fluorine orbitals is inversely proportional to the number of fluorines.

Finally, computations were carried out for the first time on the electronic excitation energies and oscillator strengths for the $CF_2{=}CF_2^-$, *c*-$C_3F_4^-$, *c*-$C_4F_6^-$ and *c*-$C_5F_8^-$ radical anions by the TD-B3LYP methods. The computations resulted in the finding of weak oscillator strengths in the visible light region, which supports the present experimental results showing that all the ESR spectral lines attributable to the radical anions are removed by exposure of the sample to unfiltered light from a tungsten lamp.

Acknowledgment. This work was supported by the Wenner-Gren Foundation (Sweden) and by the Division of Chemical Sciences, Office of Basic Energy Sciences, United States Department of Energy under Grant No. DE-FG02-88ER13852. We thank Dr. M. B. Yim for providing us with the unpublished experimental ^{19}F hyperfine splittings of *c*-$C_3F_4^-$, and Mr. Y. Umeyama, Hiroshima University, for his help in recording the ESR spectra of *c*-$C_5F_8^-$ in MTHF. We are also indebted to a referee for several helpful comments on this work.

Supporting Information Available: (1) Geometrical parameters computed for *c*-C_3F_4 and *c*-$C_3F_4^-$. (2) Geometrical parameters computed for *c*-C_4F_6 and *c*-$C_4F_6^-$. (3) Electron energies and oscillator strengths computed for $C_2F_4^-$, *c*-$C_3F_4^-$, *c*-$C_4F_6^-$ and *c*-$C_5F_8^-$. This material is available free of charge via the Internet at http://pubs.acs.org.

References and Notes

(1) Green, S. W.; Slinn, D. S. L.; Simpson, R. N. F.; Woytek, A. J. In *Organofluorine Chemistry, Principles and Commercial Applications*; Banks, R. E., Smart, B. E., Tatlow, J. C., Eds.; Plenum: New York, 1994; p 89.

(2) Barthe-Rosa, L. P.; Gladysz, J. A. *Coord. Chem. Rev.* **1999**, *190*, 587.

(3) (a) Takahashi, K.; Ithoh, A.; Nakamura, T.; Tachibana, K. *Thin Solid Films* **2000**, *374*, 303. (b) Tachi, S. *J. Vac Sci. Technol.* **2003**, *A21*, S131.

(4) (a) Hiraoka, K.; Takao, K.; Iino, T.; Nakagawa, F.; Suyama, H.; Mizuno, T.; Yamabe, S. *J. Phys. Chem.* **2002**, *106*, 603. (b) Hiraoka, K.; Fujita, K.; Ishida, M.; Okada, K.; Hizumi, A.; Wada, A.; Yamabe, S.; Tsuchida, N. *J. Phys. Chem.* **2005**, *109*, 1049.

(5) Winstead, C.; McKoy, V. *J. Chem. Phys.* **2001**, *114*, 7407.

(6) Paul, A.; Wannere, C. S.; Kasalova, V.; Schleyer, P. v. R.; Schaefer, H. F., III. *J. Am. Chem. Soc.* **2005**, *127*, 15457.

(7) Shiotani, M.; Williams, F. *J. Am. Chem. Soc.* **1976**, *198*, 4006.

(8) Hasegawa, A.; Shiotani, M.; Williams, F. *Faraday Discuss. Chem. Soc.* **1977**, *63*, 157.

(9) ElSohly, A. M.; Tschumper, G. S.; Crocombe, R. A.; Wang, J. T.; Williams, F. *J. Am. Chem. Soc.* **2005**, *127*, 10573.

(10) McNeil, R. I.; Shiotani, M.; Williams, F.; Yim, M. B. *Chem. Phys. Lett.* **1977**, *51*, 433. Although the experimental ESR data for $CF_2{=}CF_2^-$ were first interpreted in this 1977 paper in terms of a σ^* (rather than a π^*) planar structure, it was also recognized that: "the EPR paramters do not rule out a chair (C_{2h}) structure if the bending of the CF_2 groups introduces only a small distortion from planarity".

(11) McNeil, R. I.; Shiotani, M.; Williams, F.; Yim, M. B. *Chem. Phys. Lett.* **1977**, *51*, 438.

(12) Morton, J. R.; Preston, K. F.; Wang, J. T.; Williams, F. *Chem. Phys. Lett.* **1979**, *64*, 71.

(13) Paddon-Row: M. N.; Rondan, N. G.; Houk, K. N.; Jordan, K. D. *J. Am. Chem. Soc.* **1982**, *104*, 1143.

(14) Hasegawa, A.; Symons, M. C. R. *J. Chem. Soc., Faraday Trans. 1* **1983**, *79*, 1565.

(15) (a) Shchegoleva, L. N.; Bilkis, I. L.; Schastnev, P. V. *Zh. Strukt. Khim.* **1984**, *25*, 19 (Russian). (b) Schastnev, P. V.; Shchegoleva, L. N. *Molecular Distortions in Ions and Excited States*; CRC Press: Boca Raton, FL, 1995; Chapter 3, pp 61−72.

(16) Hasegawa, A. In *Radical Ionic Systems: Properties in Condensed Phases*; Lund, A., Shiotani, M., Eds.; Kluwer Academic Publishers: Dordrecht, The Netherlands, 1991; p 313.

(17) Shiotani, M.; Yoshida, H. In *CRC Handbook of Radiation Chemistry*; Tabata, Y., Ed.; CRC Press: Boca Raton, FL, 1991; pp 440−467.

(18) Hou, X.-J.; Huang, M.-B. *J. Phys. Chem. A* **2002**, *106*, 10655.

(19) McNeil, R. I.; Williams, F.; Yim, M. B. *Chem. Phys. Lett.* **1979**, *61*, 293.

(20) Wang, J. T.; Williams, F. *J. Am. Chem. Soc.* **1981**, *103*, 29.

(21) Yim, M. B.; Wood, D. E. *J. Am. Chem. Soc.* **1976**, *98*, 2053.

(22) Symons, M. C. R.; Selby, R. C.; Smith, I. G.; Bratt, S. W. *Chem. Phys. Lett.* **1977**, *48*, 100.

(23) Wang, J. T.; Williams, F. *Chem. Phys. Lett.* **1980**, *71*, 471.

(24) Hasegawa, A.; Shiotani, M.; Hama, Y. *J. Phys. Chem.* **1994**, *98*, 1834.

(25) Hou, X.-J.; Huang, M.-B. *J. Mol. Structure (THEOCHEM)* **2003**, *638*, 209.

(26) Fessenden, R. W. *J. Chem. Phys.* **1962**, *37*, 747.

(27) (a) Chachaty, C.; Forchioni, A.; Shiotani, M. *C. R. Acad. Sci., Paris, Ser. C* **1969**, *268*, 1181. (b) Chachaty, C.; Forchioni, A.; Shiotani, M. *Can. J. Chem.* **1970**, *48*, 435. (c) Chachaty, C.; Shiotani, M. *J. Chim. Phys.* **1971**, *66*, 300.

(28) Chen, K. S.; Krusic, P. J.; Meakin, P.; Kochi, J. K. *J. Phys. Chem.* **1974**, *78*, 2014.

(29) Maruani, J.; McDowell, C. A.; Nakajima, H.; Raghunatthan, P. *Mol. Phys.* **1968**, *14*, 349.

(30) Maruani, J.; Coope J. A. R.; McDowell, C. A. *Mol. Phys.* **1970**, *18*, 165.

(31) Edlund, O.; Lund, A.; Shiotani, M.; Sohma, J.; Thuomas, K. A. *Mol. Phys.* **1976**, *32*, 49.

(32) Shiotani, M. In *CRC Handbook of Radiation Chemistry*; Tabata, Y., Ed.; CRC Press: Boca Raton, FL, 1991; pp 544−567.

(33) Shiotani, M. *Magn. Reson. Rev.* **1987**, *12*, 333.

(34) Hasegawa, A.; Symons, M. C. R. *Faraday Trans. 1* **1983**, *79*, 93.

(35) Shiotani, M.; Kawazoe, H.; Sohma, J. *Chem. Phys. Lett.* **1984**, *111*, 254.

(36) Shiotani, M.; Kawazoe, H.; Sohma, J. *J. Phys. Chem.* **1984**, *88*, 2220.

(37) Ohta, K.; Shiotani, M.; Sohma, J. *Chem. Phys. Lett.* **1987**, *140*, 148.

(38) Hasegawa, A.; Itagaki Y.; Shiotani, M. *J. Chem. Soc., Perkin Trans. 2* **1997**, 1625.

(39) Itagaki, Y.; Shiotani, M.; Hasegawa, A.; Kawazoe, H. *Bull. Chem. Soc. Jpn.* **1998**, *71*, 2547.

(40) Li, W.-Z.; Huang, M.-B. *J. Mol. Struct. (THEOCHEM)* **2003**, *636*, 71.

(41) Moon B. Yim, private communication.

(42) Frisch, M. J.; Trucks, G. W.; Schlegel, H. B.; Scuseria, G. E.; Robb, M. A.; Cheeseman, J. R.; Montgomery, J. A., Jr.; Vreven, T.; Kudin, K. N.; Burant, J. C.; Millam, J. M.; Iyengar, S. S.; Tomasi, J.; Barone, V.; Mennucci, B.; Cossi, M.; Scalmani, G.; Rega, N.; Petersson, G. A.; Nakatsuji, H.; Hada, M.; Ehara, M.; Toyota, K.; Fukuda, R.; Hasegawa, J.; Ishida, M.; Nakajima, T.; Honda, Y.; Kitao, O.; Nakai, H.; Klene, M.; Li, X.; Knox, J. E.; Hratchian, H. P.; Cross, J. B.; Bakken, V.; Adamo, C.; Jaramillo, J.; Gomperts, R.; Stratmann, R. E.; Yazyev, O.; Austin, A. J.; Cammi, R.; Pomelli, C.; Ochterski, J. W.; Ayala, P. Y.; Morokuma, K.; Voth, G. A.; Salvador, P.; Dannenberg, J. J.; Zakrzewski, V. G.; Dapprich, S.; Daniels, A. D.; Strain, M. C.; Farkas, O.; Malick, D. K.; Rabuck, A. D.; Raghavachari, K.; Foresman, J. B.; Ortiz, J. V.; Cui, Q.; Baboul, A. G.; Clifford, S.; Cioslowski, J.; Stefanov, B. B.; Liu, G.; Liashenko, A.; Piskorz, P.; Komaromi, I.; Martin, R. L.; Fox, D. J.; Keith, T.; Al-Laham, M. A.; Peng, C. Y.; Nanayakkara, A.; Challacombe, M.; Gill, P. M. W.; Johnson, B.; Chen, W.; Wong, M. W.; Gonzalez, C.; Pople, J. A. *Gaussian 03*, revision B.05; Gaussian, Inc.: Wallingford, CT, 2004.

(43) Lund, A. *Appl. Magn. Reson.* **2004**, *26*, 365.

(44) Lund A.; Gustafsson, H.; Maruani, J.; Shiotani, M. *Spectrochim. Acta A* **2006**, *63*, 830.

(45) Fessenden, R. W.; Schuler, R. H. *J. Chem. Phys.* **1965**, *43*, 2704.

(46) Atherton, N. M. *Principles of Electron Spin Resonance*; Ellis Horwood: New York, 1993; p 188.

(47) Abdo, B. T.; Alberts, I. L.; Attfield, C. J.; Banks, R. E.; Blake, A. J.; Brain, P. T.; Cox, A. P.; Pulham, C. R.; D. W. H.; Robertson, H. E.; Murtagh, V.; Heppeler, A.; Morrison, C. *J. Am. Chem. Soc.* **1996**, *118*, 209.

(48) Chang, C. H.; Porter, R. F.; Bauer, S. H. *J. Mol. Struct.* **1971**, *7*, 89.

(49) Xu, L. W.; Klausner, M, E.; Andrews A. M.; Kuczkowski, R. L. *J. Phys. Chem.* **1993**, *97*, 10346.

(50) Chang, C. H.; Bauer, S. H. *J. Phys. Chem.* **1971**, *75*, 1685.

(51) Brundle, C. R.; Robin, M. N.; Kuebler, N. A.; Basch, H. *J. Am. Chem. Soc.* **1972**, *94*, 1451.
(52) Houk, K. N. *J. Am. Chem. Soc*. **1979**, *101*, 1140.
(53) (a) Kasai, P. H. *J. Am. Chem. Soc*. **1982**, *104*, 1165. (b) Kasai, P. H. *J. Am. Chem. Soc*. **1992**, *114*, 3299.
(54) Matsuura, K.; Muto, H. *J. Phys. Chem.* **1993**, *97*, 8842.
(55) Itagaki, Y.; Shiotani, M. *J. Phys. Chem. A* **1999**, *103*, 5189.
(56) Weil, J. A.; Bolton, J. R.; Wertz, J. E. *Electron Paramagnetic Resonance*; John Wiley & Sons: New York, 1994; p 125.
(57) For example, Gallivan J. B.; Hamill, W. H. *J. Chem. Phys*. **1974**, *78*, 2014.
(58) (a) Goodman, B. A.; Raynor, J. *Adv. Inorg. Chem. Radiochem*. **1970**, *3*, 135. (b) Morton, J. R.; Preston, K. F. *J. Magn. Reson.* **1978**, *30*, 577.